Article

Tuft cells act as regenerative stem cells in the human intestine

Lulu Huang[1,2,9], Jochem H. Bernink[1,3,9 ✉], Amir Giladi[1,2,9], Daniel Krueger[1], Gijs J. F. van Son[1,4], Maarten H. Geurts[1,4], Georg Busslinger[1], Lin Lin[1,4], Harry Begthel[1], Maurice Zandvliet[5], Christianne J. Buskens[6], Willem A. Bemelman[6], Carmen López-Iglesias[7], Peter J. Peters[7] & Hans Clevers[1,2,4,8 ✉]

In mice, intestinal tuft cells have been described as a long-lived, postmitotic cell type. Two distinct subsets have been identified: tuft-1 and tuft-2 (ref. 1). By combining analysis of primary human intestinal resection material and intestinal organoids, we identify four distinct human tuft cell states, two of which overlap with their murine counterparts. We show that tuft cell development depends on the presence of Wnt ligands, and that tuft cell numbers rapidly increase on interleukin-4 (IL-4) and IL-13 exposure, as reported previously in mice[2–4]. This occurs through proliferation of pre-existing tuft cells, rather than through increased de novo generation from stem cells. Indeed, proliferative tuft cells occur in vivo both in fetal and in adult human intestine. Single mature proliferating tuft cells can form organoids that contain all intestinal epithelial cell types. Unlike stem and progenitor cells, human tuft cells survive irradiation damage and retain the ability to generate all other epithelial cell types. Accordingly, organoids engineered to lack tuft cells fail to recover from radiation-induced damage. Thus, tuft cells represent a damage-induced reserve intestinal stem cell pool in humans.

The human intestinal tract is responsible for nutrient uptake and the production of hormones, while protecting against pathogens. These functions are executed by specialized epithelial cells, generated by LGR5+ stem cells[5]. Tuft cells represent one such specialized epithelial subset. Most insights in tuft cell ontology and function derive from mouse studies because of a paucity of human in vitro tuft cell models. Mouse tuft-1 cells express neuronal-type genes, whereas tuft-2 cells appear primarily involved in protective immunity against helminths, protozoans and bacteria[6–9]. Murine tuft cells express the cytokine IL-25, which triggers resident type 2 innate lymphoid cells (ILC2s) to secrete IL-13. This cytokine is thought to signal to the LGR5+ stem cells and to uncommitted progenitor cells to promote the de novo generation of tuft cells in a positive feedback loop[2–4]. Tuft-2 cells sense microbe-derived metabolic compounds, resulting in enhanced secretion of arachidonic acid-derived lipid mediators, such as prostaglandins and leukotrienes, that in turn activate IL-13-producing ILC2s and mucus-secreting goblet cells[8,9].

Although LGR5+ cells represent the 'workhorse' stem cells of the intestinal epithelium[5], they are highly susceptible to damage and various mechanisms can compensate for stem cell loss in mice. One such mechanism involves plasticity of fated crypt progenitors. Thus, dedifferentiation of secretory progenitors[10–13] and enterocyte progenitors[14]

can restore normal numbers of LGR5+ stem cells. Also, a subpopulation of quiescent LGR5+ stem cells marked by MEX3A can restore stem cell function[15]. Finally, so-called revival stem cells, defined by transient induction of clusterin (CLU) and SCA1, have been proposed to be key to intestinal regeneration, although it is not known from which cells these revival stem cells derive[16,17]. The lack of models to study human tuft cell biology impedes the functional characterization and properties of these cells in detail, and human intestinal regenerative stem cells have yet to be identified.

Wnt supports human tuft cell development

To generate a model for visualization and tracking of human intestinal tuft cell dynamics and function, we mined a published single-cell RNA sequencing (scRNA-seq) resource to select markers that are uniformly, yet specifically, expressed among human tuft cells[18]. We thus identified *AVIL*, a gene encoding for the structural actin-binding protein advillin, to be highly expressed in tuft cells and not in other intestinal epithelial cells (more than 192-fold higher expression than any other epithelial type; Fig. 1a), as previously also documented for murine tuft cells[19,20]. Histological examination confirmed the specificity of AVIL expression in primary human small intestinal and colon tissue (Extended Data Fig. 1a).

[1]Hubrecht Institute, Royal Netherlands Academy of Arts and Sciences (KNAW) and University Medical Center Utrecht, Utrecht, the Netherlands. [2]Oncode Institute, Hubrecht Institute, Utrecht, the Netherlands. [3]Amsterdam University Medical Center, University of Amsterdam, Department of Experimental Immunology, Amsterdam Institute for Immunology and Infectious Diseases, Amsterdam, the Netherlands. [4]The Princess Maxima Center for Pediatric Oncology, Utrecht, the Netherlands. [5]Department of Clinical Sciences of Companion Animals, Faculty of Veterinary Medicine, Utrecht University, Utrecht, the Netherlands. [6]Amsterdam University Medical Center, University of Amsterdam, Department of Surgery, Amsterdam Gastroenterology Endocrinology Metabolism, Amsterdam, the Netherlands. [7]The Maastricht Multimodal Molecular Imaging Institute, Maastricht University, Maastricht, the Netherlands. [8]Present address: Pharma, Research and Early Development of F. Hoffmann-La Roche Ltd, Basel, Switzerland. [9]These authors contributed equally: Lulu Huang, Jochem H. Bernink, Amir Giladi. ✉e-mail: j.h.bernink@amsterdamumc.nl; h.clevers@hubrecht.eu
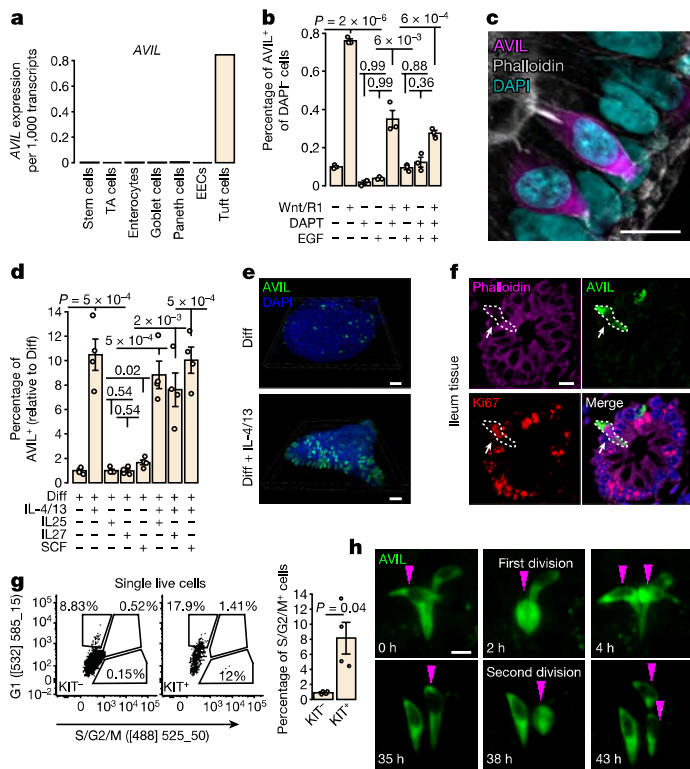
Fig. 1 | Wnt and IL-4 drive tuft cell differentiation and proliferation. a, *AVIL* expression in a scRNA-seq dataset of human adult small intestinal tissue[18]. $n = 15,184$ single epithelial cells. **b**, Flow cytometric quantification of the AVIL-Clover[+] cell percentage of DAPI^{−} cells cultured in differentiation regimens. Each dot is a well. $n = 3$ wells per condition. Results are representative of three independent experiments (Supplementary Fig. 1b). **c**, Differentiated human ileum AVIL-Clover organoids counterstained with phalloidin (F-actin). Three independent experiments were performed on two donors with similar results. **d**, Flow cytometric quantification of AVIL[+] cell frequency in AVIL-Clover reporter organoids, differentiated with indicated recombinant proteins. Values are normalized to human tuft cell differentiation medium levels. Each dot represents one well. $n = 4$ wells per condition. Results are representative of four individual donors (Supplementary Fig. 1c). **e**, Fluorescence images of AVIL-Clover organoids differentiated with or without IL-4/IL-13. $n = 3$ independent experiments. **f**, Costaining of AVIL, Ki67 and phalloidin in human ileum tissue. $n = 3$ donors (Extended Data Fig. 2k). Arrows and dashed lines indicate cells showing AVIL-Ki67 overlap. **g**, Representative flow cytometry (left) and quantification (right) of the S/G2/M fraction in KIT[−] or KIT^{+} cells in ileum FUCCI reporter organoids differentiated with IL-4/IL-13. Each dot is a well. $n = 4$ wells per condition (pooled from three independent experiments). **h**, Live-cell imaging snapshots of continuous divisions of AVIL^{+} cells in AVIL-Clover organoids differentiated with IL-4/IL-13 (Supplementary Video 4). $n = 2$ donors (Extended Data Fig. 3m and Supplementary Video 5). **a**,**b**,**d**,**g**, Data are presented as mean values (**a**) or as mean values ± standard error (**b**,**d**,**g**). **b**,**d**,**g**, *P* values are derived from false discovery rate (FDR)-adjusted one-tailed Student's *t*-test against the base or diff medium (**b**,**d**) or two-tailed Student's *t*-test (**g**). Scale bars, 10 μm (**c**,**f**,**h**), 50 μm (**e**). TA cells, transit-amplifying cells; R1, R-spondin1 conditioned medium; Diff, human tuft cell differentiation medium.

We generated clonal organoid lines from human duodenum, ileum and colon in which we fused a green fluorescent protein (mClover) to the C terminus of AVIL using a CRISPR-assisted non-homologous end-joining approach at the *AVIL* locus[21] (Extended Data Fig. 1b and Supplementary Fig. 1a). Following an expansion phase of 4 days, AVIL-Clover organoids were subjected to many differentiation regimens in which growth factors were added either alone or in combination (Extended Data Fig. 1c). Using flow cytometry for quantification, we observed the highest frequency of AVIL-Clover^{+} cells in the presence of

Wnt (Fig. 1b and Extended Data Fig. 1d,e). No higher tuft cell numbers were reached by blocking Notch signalling using the gamma-secretase inhibitor DAPT, whereas addition of epidermal growth factor (EGF) reduced tuft cell frequency, although these factors increased overall cell survival (Extended Data Fig. 1f). The specificity of the reporter lines was confirmed by antibody staining for endogenous AVIL (Extended Data Fig. 1g). Like primary tuft cells, organoid-derived AVIL^{+} cells were characterized by flask-shaped contours and intense bundling of actin fibres towards the tip of the tuft (Fig. 1c and Extended Data Fig. 1h). Electron microscopy imaging further revealed that, like primary tuft cells, organoid-derived tuft cells formed distinctive lateral protrusions or interdigitating spinules[22] (Extended Data Fig. 1i). In agreement with these observations, AVIL^{+} cells expressed high levels of previously described signature tuft cell genes[18] as demonstrated by quantitative polymerase chain reaction (qPCR) and staining in organoids and primary tissue (Extended Data Fig. 1j–n).

High Wnt levels are present in the intestinal crypts, and inversely correlate with bone morphogenic protein (BMP) signalling, the latter being a key driver of epithelial differentiation, predominantly active in the intestinal villi[23]. Removal of the BMP inhibitor Noggin and addition of BMP2 and BMP4 to differentiating organoids reduced tuft cell frequency (Extended Data Fig. 2a,b). The observed dependence on Wnt and on BMP inhibition urged us to explore the cellular localization of tuft cells in the human intestine. Indeed, quantifying tuft cells along the crypt–villus axis in the primary human small intestine tissue showed that these cells are predominantly restricted to the crypt area (Extended Data Fig. 2c,d).

IL-4 drives tuft cell proliferation

Elevated levels of intestinal IL-4 and IL-13, cytokines related to type 2 immunity, drive tuft cell hyperplasia in mice, proposedly by increasing de novo generation of tuft cells by LGR5^{+} stem cells[2–4]. We explored cytokine receptor expression profiles in human intestinal epithelial lineages. Tuft cells (rather than stem cells) expressed the highest level of *IL13RA1*, the gene encoding the shared IL-4 and IL-13 receptor (Extended Data Fig. 2e). A 4-day exposure of intestinal organoids to IL-4 and IL-13 (but not to IL-25, IL-27 or SCF (KIT ligand)) induced a 10- to 15-fold increase in AVIL[+] cell frequency, most evident in the absence of EGF (Fig. 1d and Extended Data Fig. 2f,g). These results raised the question of whether proliferation of bona fide tuft cells, rather than differentiation of stem or transit-amplifying cells to tuft cells, is the main driver of elevated tuft cell numbers following exposure to IL-4 and IL-13. Notably, imaging of IL-4/IL-13-treated organoids revealed a pattern of clustered tuft cells, suggestive of self-expansion, whereas untreated organoids yielded a more scattered profile (Fig. 1e and Extended Data Fig. 2h,i). Moreover, a substantial fraction of IL-4/IL-13-induced tuft cells stained for Ki67, pointing towards local proliferation of differentiated tuft cells (Extended Data Fig. 2j and Supplementary Video 1). These findings were not restricted to in vitro models, as staining in primary human small intestinal tissues also sporadically marked Ki67 signal within AVIL[+]GNAT3^{+} cells (Fig. 1f and Extended Data Fig. 2k–o).

To further substantiate these findings, we integrated the fluorescent ubiquitination cell cycle indicator (FUCCI)[24] in small intestine organoids using a transposon-based system, allowing to track and quantify the mitotic state in organoids. We identified KIT as a tuft cell-specific surface marker (Extended Data Figs. 2e and 3a–d), showing a more than 98% overlap in three AVIL-Clover reporter organoid lines (Extended Data Fig. 3e). This overlap was maintained following exposure to various stimuli (Extended Data Fig. 3f,g), confirming KIT as a robust antigen that specifically marks tuft cells among human intestinal epithelial cells. We further confirmed KIT specificity in both healthy and inflamed intestines, by analysing publicly available scRNA-seq data of human colon epithelium, obtained from a cohort of paediatric and

adult healthy and inflammatory bowel disease tissues[25] (Extended Data Fig. 3h). Likewise, scRNA-seq of KIT-sorted cells from human adult ileum and colon primary tissue revealed that more than 97% of sorted cells showed a tuft cell transcriptional signature (Extended Data Fig. 3i,j). Thus, KIT specificity allowed us to simultaneously stain tuft cells and track their cell cycle progression with the FUCCI construct by flow cytometry analysis.

Following IL-4 and IL-13 stimulation, up to 8% of the KIT^+ fraction entered the S/G2/M-phase, whereas the KIT^- fraction remained quiescent (less than 1% cycling) (Fig. 1g). Of note, non-cytokine-exposed tuft cells were occasionally found in the S/G2/M-phase (Extended Data Fig. 3k and Supplementary Video 2). Using live-cell imaging, we observed IL-4/IL-13-stimulated $AVIL^+$ cells that divided twice over a 36-hour period (Fig. 1h, Extended Data Fig. 3l,m and Supplementary Videos 3–5). In agreement with these findings, IL-4/IL-13 stimulation promoted continuous cycling of tuft cells, as determined using FUCCI organoids (Supplementary Fig. 1l) and a steady increase in $Ki67^+AVIL^+$ cell frequency over a 7-day period (Extended Data Fig. 3n). These processes were enhanced in the presence of Wnt signalling (Extended Data Fig. 3o). Exposure of IL-4 and IL-13 to organoids that did not contain tuft cells (that is, organoids differentiated in the absence of Wnt), did not result in tuft cell expansion (Extended Data Fig. 3p), neither did we observe tuft cells in sorted and cultured stem cells in expansion medium in the presence of IL-4 and IL-13 over a 7-day period (Extended Data Fig. 3q). This uncoupled IL-4/IL-13-induced tuft cell proliferation from induced differentiation of precursor cells. Taken together, we found tuft cells to be capable of robust proliferation following type 2 cytokine stimulation in situ.

IL-4 shifts tuft cell substate balance

To gain a better understanding of tuft cell function and heterogeneity, we obtained scRNA-seq data from 953 ileum organoid-derived epithelial cells, cultured in tuft cell differentiation medium with and without exposure to IL-4/IL-13. We used the AVIL-Clover signal to select for tuft cells, resulting in 580 high-quality AVIL-expressing cells and 373 cells from other epithelial lineages (Extended Data Fig. 4a–c). The MetaCell package[26] grouped cells into transcriptionally homogeneous subsets, identifying four distinct clusters, which we succinctly named tuft-1 to tuft-4 (Fig. 2a,b). Non-tuft cells were identified as $LGR5^+$ stem cells and two types of goblet cell (Extended Data Fig. 4d). All four tuft cell clusters shared a unique tuft cell core gene-expression program (absent from the non-tuft cell fraction), including the genes ALOX5AP, POU2F3, LRMP, GNG13, BMX, AVIL, GNAT3 and KIT (Fig. 2c and Extended Data Fig. 4e). We also identified genes not previously linked to tuft cells, such as the neuropeptide neuromedin U (NMU), and the tyrosine-protein kinase HCK (Fig. 2c). Relative tuft cell subset distribution largely depended on medium composition: addition of IL-4 and IL-13 caused a shift towards tuft-3 and tuft-4 (comprising 14.25% and 79% of all IL-4/IL-13-stimulated tuft cells, respectively), whereas under 'homeostatic' differentiation conditions these populations were much rarer (3.5% and 3.25%; Fig. 2d). Note that the ratio of tuft cell substates was determined within treatment groups, and that the absolute number of tuft cells within IL-4/IL-13-treated organoids was roughly 10- to 20-fold higher than within non-cytokine-treated organoids (Fig. 1d). Direct comparison of the individual tuft cell substates to other epithelial cells showed unique and shared gene-expression patterns for each subset, with tuft-3 expressing the largest number (more than 250) of unique differentially expressed genes (DEGs), followed by tuft-2 and tuft-4 (Extended Data Fig. 4f).

Gene ontology analysis of the DEGs within each tuft cell cluster highlighted the diversity between tuft-1 to tuft-4 (Extended Data Fig. 4g). For example, genes that were enriched in tuft-1 cells are involved in processes of neuron differentiation (for example, VIM and SEMA3C), and tuft-2 genes are involved in immuno-potent lipid biosynthetic

processes such as the synthesis of lipoxins, prostaglandins and cysteinyl-leukotrienes. Tuft-3 is enriched for genes connected to a cycling phenotype, with high gene-expression levels of MKI67, TOP2A, TUBB and CKS1B, and tuft-4 cells express genes that are involved in regulating immune responses and stimulating regeneration, such as genes encoding the SOCS proteins, PD-L1 (CD274), EREG, HB-EGF and TACSTD2, among others (Fig. 2e). Staining AVIL-Clover reporter organoids with tuft cell state-specific markers further confirmed the observed tuft cell heterogeneity (Extended Data Fig. 4h).

We next asked whether the heterogeneity we observed in organoid tuft cells informed on tuft cell heterogeneity in vivo. In our dataset of KIT-sorted tuft cells from human adult ileum and colon primary tissue, we found a small subset of cells showing a large repertoire of tuft-3 genes, indicating that tuft cells enter the cell cycle in vivo (Extended Data Fig. 4i,j). Combining 2 published datasets spanning 14 healthy donors[18,27], we estimated that 3.9% of intestinal tuft cells are cycling in steady state (Extended Data Fig. 4k). We also detected coordinated expression of tuft-4 genes in a gradient-like manner in primary ileum and colon tuft cells, suggesting variable levels of IL-4/IL-13 activation in the homeostatic intestine (Extended Data Fig. 4l–m). We noted that tuft-3 cells in vivo show a significantly higher tuft-4 activation signature compared to other tuft cells, linking tuft cell proliferation to cytokine stimulation, similar to our observations in vitro (Extended Data Fig. 4n,o).

Taken together, we observed heterogeneity within the human intestinal tuft cell lineage. At steady state, the predominant subsets represent tuft-1 and tuft-2, which phenocopied the two previously described murine intestinal crypt tuft cell subsets[1]. IL-4 signalling triggered induction of cycling tuft-3 cells and the notable expansion of tuft-4, the latter not recognized in mouse and probably involved in immune regulation and/or epithelial renewal.

Next, we explored the transcription factor repertoire of tuft cells, identifying POU2F3, among others, to be uniquely and uniformly expressed by tuft cells in intestinal organoids and tissue (Extended Data Fig. 5a,b). Using conventional CRISPR–Cas9 and base-editing techniques[28], we generated knock-outs of prominent tuft cell-expressing transcription factors in AVIL-Clover reporter organoids (Extended Data Fig. 5c) and tested their effect on tuft cell frequency by flow cytometry (Extended Data Fig. 5d). By quantifying tuft cell frequency in 'homeostatic' differentiation medium and IL-4/IL-13-induced medium, we observed that POU2F3 and the Wnt-signal transducer TCF7 are essential for tuft cell development (Fig. 2f and Extended Data Fig. 5e). Accordingly, POU2F3 colocalized with AVIL in sections of organoids generated from small and large intestines, as well as at the transcript and protein levels in primary intestinal tissue (Fig. 2g,h and Extended Data Fig. 5f–h). Knocking out SPIB, a transcription factor that is shared with M cells and $BEST4^+$ cells[18,29], partially reduced tuft cell numbers. In addition, we found that organoids mutant for HMX2 retained normal tuft cell numbers when cultured in homeostatic differentiation medium, but essentially lost the tuft cell proliferation response to IL-4 and IL-13, consistent with the differential expression of HMX2 in tuft-3 and tuft-4 (Fig. 2f and Extended Data Fig. 5a). Of note, several conflicting studies in mice reported tuft cell dependence on the secretory lineage-defining transcription factor ATOH1 (ref. 30). We did not detect ATOH1 expression in human tuft cells, and ectopic overexpression of ATOH1 in AVIL-Clover reporter organoids had a negative effect on tuft cell frequency (Extended Data Fig. 5i,j). Of note, ATOH1 overexpression induced goblet cells and Paneth cells but not enteroendocrine cells (EECs) (Extended Data Fig. 5k). Paradoxically, knocking out ATOH1 resulted in a strong reduction in tuft cell frequency, whereas IL-4/IL-13-induced tuft cell proliferation was not affected (Extended Data Fig. 5l–n). Analysis of tuft cell-state-specific markers did not point towards the loss of a specific subset (Extended Data Fig. 5o). Thus, ATOH1 appears to be instrumental in a developmental phase towards tuft cells, but dispensable for tuft cell maintenance. Taken together,
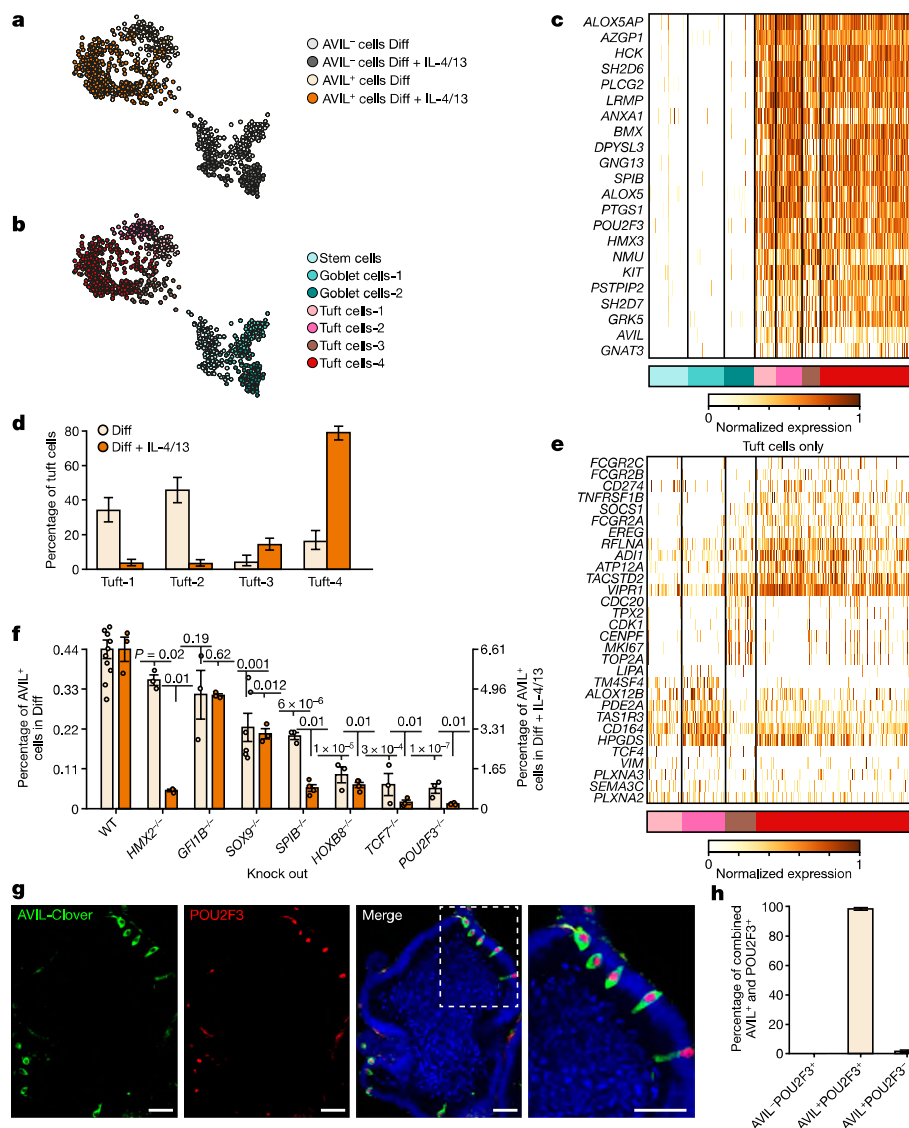
Fig. 2 | IL-4 signalling shifts the balance in tuft cell states. a,b, MetaCell 2D projection of 953 ileum organoid-derived single cells. Cells are coloured by their gating and medium condition (**a**) or by annotation to cell subsets (**b**). **c**, Gene-expression profiles of tuft cell-specific core genes shared by all tuft cell clusters across epithelial subsets. **a–c**, $n = 953$ single cells. **d**, Distribution of the four tuft cell states in ileum-derived organoids with or without IL-4/IL-13. **e**, Gene-expression profiles of tuft cell state-specific genes. **d,e**, $n = 573$ single tuft cells. **f**, Flow cytometry quantification of AVIL$^+$ cell frequency in organoid mutant lines of selected transcription factors (homozygous knock-outs). Organoids were differentiated for 11 days (or 6 days with IL-4/IL-13).

Each dot is one well. $n = 11$ (WT Diff), 6 ($SOX9^{-/-}$ Diff), 4 ($SPIB^{-/-}$/$HOXB8^{-/-}$/$POU2F3^{-/-}$ Diff + IL-4/13) and 3 (rest) wells. Results are representative of three independent experiments (Supplementary Fig. 2a). P values are derived from FDR-adjusted two-tailed Student's t-test against the WT levels. **g,h**, Representative fluorescence image (**g**) and quantification (**h**) of AVIL-Clover organoids costained for POU2F3. **g**, $n = 3$ donors (Supplementary Fig. 2b and Supplementary Videos 6–8). Scale bars, 40 μm. **h**, $n = 993$ positive cells from 17 organoids pooled from three donors. **d,f,h**, Data are presented as binomial estimation of the mean ± 95% confidence intervals (**d**) or as mean values ± standard error (**f,h**).

we identified four tuft cell states, which developed in a *POU2F3*- and *TCF7*-dependent manner, whereas IL-4/IL-13-induced tuft cell expansion depended on *HMX2*.

Single tuft cells give rise to organoids

Given the capacity of the tuft cells to expand, we next explored their organoid-forming potential. We purified S/G2/M$^+$ tuft cells and non-tuft cells from IL-4- and IL-13-treated FUCCI organoids (Extended Data Fig. 6a). Small spheroids appeared from sorted single KIT$^+$ cells at day 3 when cultured in expansion medium (Fig. 3a). Following passaging, tuft cell-derived organoids appeared larger than non-tuft cell-derived organoids (Extended Data Fig. 6b). Similar results were obtained with sorted organoid-derived single AVIL$^+$ cells and adult tissue-derived KIT$^+$

cells (Extended Data Fig. 6c,d), albeit at a lower frequency, probably as it contained all tuft cell states rather than proliferating tuft cells only. Of note, following seeding, AVIL$^+$ cells rapidly downregulated tuft cell-specific genes such as *AVIL* and upregulated stem cell markers such as *LGR5* (Extended Data Fig. 6e).

In expansion medium and following differentiation, either with or without IL-4 and IL-13, tuft cell- (as determined by expression of KIT or AVIL) and non-tuft cell-derived organoids showed similar expression levels of genes that define absorptive enterocytes (*FABP1*), goblet cells (*MUC2*), tuft cells (*AVIL*) and stem cells (*LGR5*) (Extended Data Fig. 6f). However, tuft cell-derived organoids expressed higher levels of the EEC marker *CHGA* in differentiation medium without IL-4 and IL-13, which was subsequently confirmed by histological analysis (Extended Data Fig. 6g).
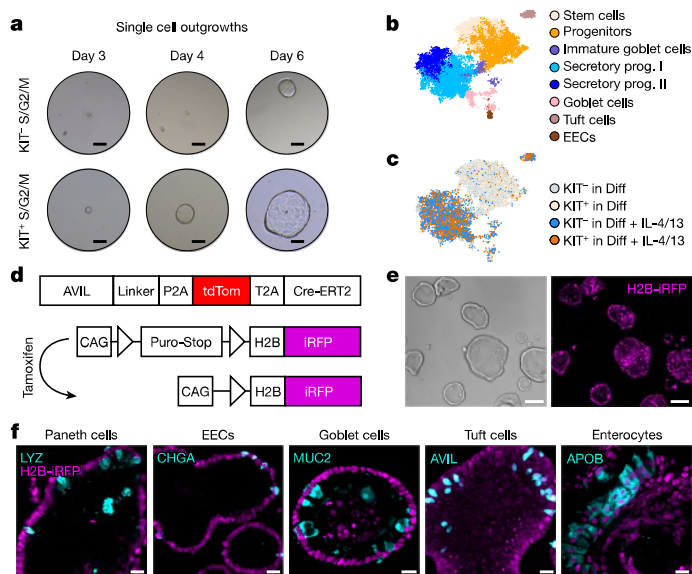
Fig. 3 | Single tuft cells give rise to organoids containing all epithelial lineages. a, Organoid outgrowth of single S/G2/M-phase KIT⁻ and KIT⁺ cells sorted from ileum FUCCI reporter organoids, cultured in standard human intestinal expansion medium. n = 3 independent experiments. **b,c**, MetaCell 2D projection of 10,311 single cells isolated from passage 1 KIT⁻ and KIT⁺ cell-derived organoids, differentiated with or without IL-4/IL-13. Cells are coloured by cell-type annotation (**b**) or by medium condition and organoid founder cell (**c**). **d**, AVIL lineage-tracing strategy in human organoids. **e**, Images of AVIL lineage-tracing organoids, derived from sorted AVIL-tdT⁺iRFP⁺ cells (as in Extended Data Fig. 7m,n, day 0). **f**, Representative images of intestinal epithelial lineages markers in differentiated traced organoids. **e,f**, n = 3 independent experiments with similar results. Scale bars, 100 μm (**a,e**), 20 μm (**f**). tdTom, tdTomato.

This observed divergence in *CHGA* expression between tuft cell- and non-tuft cell-derived organoids normalized following further passaging (Extended Data Fig. 6h,i), indicating that the balance between the distinct epithelial subtypes is reestablished over time. In agreement with this, no differences in cell frequencies between passaged tuft cell- and non-tuft cell-derived organoids were detected by scRNA-seq analysis (Fig. 3b,c and Extended Data Fig. 6j,k). Of note, the depicted marker genes were highly enriched in tuft cells. For example, *AVIL*, *POU2F3* and *KIT* expression was 75-, 20- and 220-fold higher in tuft cells compared to other epithelial cell types, respectively (Extended Data Fig. 6j).

This transient effect on *CHGA* expression could not be explained by tuft cells expressing the *CHGA* gene themselves, as wild-type (WT) organoid-derived AVIL⁺ purified cells did not express *CHGA*, whereas the AVIL⁻ population did (Extended Data Fig. 7a). Indeed, imaging, as well as flow cytometry analysis of differentiated organoids, confirmed the mutually exclusive expression of AVIL against either chromogranin A or chromogranin B (Extended Data Fig. 7b–d). *POU2F3*-deficient organoids showed reduced *CHGA* expression and protein levels in tuft cell differentiation medium (Extended Data Fig. 7e–g), suggesting the involvement of tuft cells in developing and/or maintaining EEC frequency. Moreover, culture conditions that are known to enhance EEC development and maturation[31] induced *CHGA* expression only in WT organoids, and not in *POU2F3⁻/⁻* organoids (Extended Data Fig. 7h).

We formulated two alternative explanations to *CHGA* dependence on tuft cells: either tuft cells act as support cells for EEC development in a paracrine manner, or tuft cells are precursors to EECs. To address this question, we mixed cells from H2B-iRFP-labelled WT organoids (WT^Red) and *POU2F3⁻/⁻* organoids, forming mosaic organoids (Extended Data Fig. 7i–k). Following differentiation, *CHGA*, *SST* and *TPH1* expression was enriched in WT^Red+ cells, but showed low expression in the *POU2F3⁻/⁻* cells (Extended Data Fig. 7l), suggesting

a paracrine effect. We further implemented a CRISPR–Cas9-mediated organoid lineage-tracing strategy (Fig. 3d). Here, Cre^ERT2 is under the control of *AVIL* expression, driving the excision of a stop-sequence that activates a viral promotor-induced H2B-iRFP construct, following tamoxifen administration. We observed expression of iRFP⁺ cells that lost AVIL expression, representing tuft cell progeny (Extended Data Fig. 7m,n). We then proceeded to analyse organoids derived from single AVIL⁺iRFP⁺ cells (Fig. 3e and Extended Data Fig. 7m,n). These fully iRFP-labelled organoids contained all main intestinal epithelial lineages, including CHGA-expressing EECs (Fig. 3f and Extended Data Fig. 7o). Thus, in agreement with the organoid-forming potential of single tuft cells shown above, AVIL⁺ cells have stem cell-like properties.

IL-4 enhances repair by tuft cells

We found genes associated with intestinal stem cells to be highly expressed by tuft cells. These included *ASCL2*, *BMI1* and *SOX4*, but not *OLFM4* and *LGR5* (ref. 32) (Extended Data Fig. 8a,b). A few stem cell-associated genes, such as *SMOC2* and *TACSTD2*, were upregulated following IL-4 and IL-13 exposure, and were indeed upregulated in tuft-3/tuft-4 states. Furthermore, organoid-derived tuft cells expressed genes previously associated with fetal gut-like stem cells, facultative stem cells or revival stem cells, including *TACSTD2*, *MEX3A*, *PROX1* and *ANXA1* (refs. 12,15,16), of which the last two were also expressed in primary tissue (Extended Data Fig. 8a,b), suggesting a role for tuft cells in epithelial renewal following mechanical injury or other insults.

Mechanical passaging of organoids as a model to induce stress and damage did not show differences in organoid outgrowth dynamics or size between wild-type- and *POU2F3*-deficient organoids (Fig. 4a). However, mechanical disruption of differentiated organoids, followed by expansion, showed a diminished expansion potential in *POU2F3⁻/⁻* compared to WT organoids (Fig. 4b). These findings suggested a compromised regenerative capacity in organoids that lack tuft cells. To substantiate these observations, we transfected organoids with a doxycycline-inducible construct that ectopically expresses *POU2F3* under the control of a viral promoter. Indeed, ectopic *POU2F3* expression resulted in a higher frequency of KIT⁺ cells and high expression of tuft cell-related genes following differentiation, and triggered enhanced organoid area as compared to control after mechanical disruption (Extended Data Fig. 8c–e). Fast-cycling cells, including stem cells, are vulnerable to irradiation damage. Hence, we irradiated differentiated organoids (5–6 Gy), followed by a 2-day IL-4 and IL-13 pulse (and a non-pulsed control), after which the organoids were allowed to expand (Fig. 4c). After an expansion phase of 2 weeks, *POU2F3⁻/⁻* organoids gradually lost their potential to passage or expand (Fig. 4d). Wild-type organoids recovered from differentiation and irradiation, and this effect was stronger in organoids that had been exposed to IL-4 and IL-13 (Fig. 4e,f). To further explore whether tuft cells have a major role in reconstitution following injury, we irradiated organoids harbouring the AVIL lineage-tracing construct (Fig. 4g and Extended Data Fig. 8f,g). After a recovery period of 9 days, we detected iRFP labelling of entire organoid segments, as well as an overall increase in labelled cell frequency, further confirming the regenerative capacity of tuft cells in these settings (Fig. 4h,i).

Epithelial renewal depends on the presence of growth factors. Our transcriptional analysis showed an IL-4- and IL-13-induced upregulation of epiregulin (*EREG*), and—to a lower extent—amphiregulin (*AREG*) and heparin binding EGF (*HBEGF*) in tuft-3 and tuft-4 cells (Extended Data Fig. 8a,h). The relevance of these growth factors in the context of injury-induced epithelial regeneration was confirmed by examining irradiated organoids engineered to lack *EREG* (Extended Data Fig. 8i–k). Conversely, recombinant EREG supplementation to differentiated *POU2F3⁻/⁻* organoids partly restored organoid formation (Extended Data Fig. 8l–n). Thus, these experiments indicated that tuft cells respond to the wound-repair-associated cytokines IL-4 and IL-13
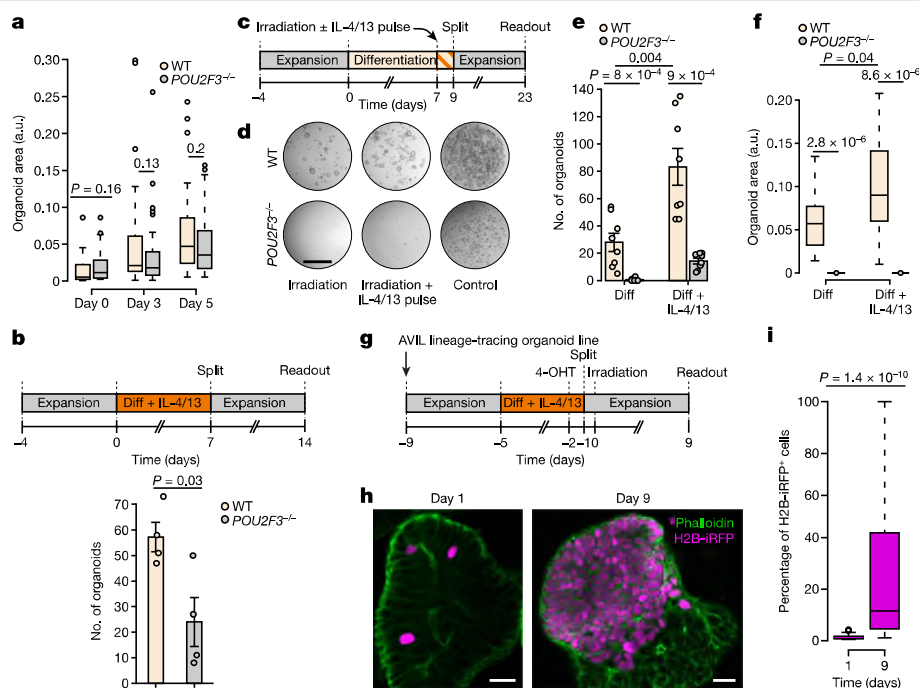
Fig. 4 | IL-4 signalling enhances the regenerative response in tuft cells.
a, Area of organoids cultured in human intestinal expansion medium following passaging at different time points. Shown is one of three independent experiments; $n = 51$ (d0 WT), 50 (d0 KO), 47 (d3 WT), 51 (d3 KO), 35 (d5 WT) and 50 (d5 KO) individual organoids. **b**, Schematic (top) of experimental set-up and quantification (bottom) of organoid numbers after mechanical damage. Each dot is a well. $n = 4$ wells per condition. Results are representative of three independent experiments on two donors (Supplementary Fig. 4a). **c–f**, Schematic (**c**), representative images (**d**), quantification of organoid numbers (**e**) and organoid areas (**f**) from organoids following irradiation and

passaging. Experiments were performed on three donors (Supplementary Fig. 4b–d). **e**, Each dot is one well. $n = 8$ wells per condition. **f**, $n = 17$ organoids per condition. **g–i**, Schematic (**g**), representative images (**h**) and quantification (**i**) of AVIL lineage-tracing organoids after irradiation. **i**, Results are pooled from three independent experiments, $n = 68$ (day 1) or 76 (day 9) organoids. **a,f,i**, Boxplots show data from the 25th to 75th percentiles and whiskers extending to the minimum and maximum within 1.5× inter-quartile range, with dots marking outliers. **b,e**, Data are presented as mean values ± standard error. **a,b,e,f,i**, P values are derived from two-tailed Student's t-test (**a,f,i**) or two-tailed Mann–Whitney test (**b,e**). Scale bars, 2 mm (**d**) and 20 μm (**h**). a.u., arbitrary units.

---

by a rapid proliferative response and the production of growth factors, whereas the concomitant dedifferentiation unleashes their reserve stem cell function.

The observed stem cell-like transcriptional profile and regenerative properties of adult tuft cells raised the question of whether tuft cells in developing intestines contribute to intestinal formation. On direct comparison to adult intestinal tissue, fetal human intestines showed an increased frequency of KIT+ cells (Extended Data Fig. 9a). Fetal KIT+ cells showed a tuft cell signature on par with adult and paediatric intestinal tuft cells as determined by single-cell sequencing, and did not express higher levels of genes associated with a stem cell phenotype (Extended Data Fig. 9b–d). Similarly, histological analysis using an antibody against AVIL confirmed the characteristic tuft cell shape (Extended Data Fig. 9e), and revealed their scattered presence throughout the villus and intervillous zones (Extended Data Fig. 9f). Cell sorting and subsequent culturing of KIT+ and KIT– cells from primary fetal intestinal specimen confirmed that these fetal tuft-like cells showed potent organoid-forming potential, by comparison to non-tuft cells (Extended Data Fig. 9g–i). The presence of tuft cells in fetal tissues suggest that these cells may be involved in the expansion of the intestinal epithelium during the fetal stages.

Discussion

Regenerative responses are frequently accompanied by increased IL-4 and IL-13 levels[33]. Mouse tuft cell numbers are known to be controlled by these cytokines[2–4]. The current study shows four human tuft cell states, with differential functions. All four states maintain a shared core tuft cell gene-expression profile. Previously reported reserve and/or

revival stem cells in mice[16,17,34] have many features in common with tuft cells described here: human tuft cells express markers linked to these previously reported facultative stem cells, such as *TACSTD2*, *ANXA1*, *BMI1* and *CLU*. This notion is further supported by a reinterpretation of early studies in mice that have linked DCLK1-expressing cells, a then unappreciated murine tuft cell marker, to proliferation in the context of a putative cancer-inducing stem cell population[35,36]. Indeed, in a study using a BAC-DCLK1::CreERT–dependent strategy to lineage-trace DCLK1-positive cells, it was observed that a small subset of DCLK1+ cells could contribute to tissue regeneration after damage as assessed by lineage tracing in vivo. In the same study, it was shown that DCLK1+ cells could grow out in short-term three-dimensional culture, expanding over a 1–2-week period[37]. From the perspective of the current study, we would interpret these combined data to indicate an evolutionary conserved capacity of tuft cells to act as reserve and/or revival stem cells in the context of intestinal injury.

Taken together, the observations in this study may have implications for regenerative medicine, opening up strategies for therapeutic interventions involving interleukins such as IL-4 and IL-13. Although the current study is focused on the intestinal tract, tuft cells are widely present in other endoderm-derived tissues[38]. It would be of interest to study the potential regenerative roles of tuft cells in tissues, such as the bile ducts, urinary tract and airways.

Online content

Any methods, additional references, Nature Portfolio reporting summaries, source data, extended data, supplementary information, acknowledgements, peer review information; details of author contributions

and competing interests; and statements of data and code availability are available at https://doi.org/10.1038/s41586-024-07952-6.

1. Haber, A. L. et al. A single-cell survey of the small intestinal epithelium. *Nature* **551**, 333–339 (2017).
2. von Moltke, J., Ji, M., Liang, H. E. & Locksley, R. M. Tuft-cell-derived IL-25 regulates an intestinal ILC2-epithelial response circuit. *Nature* **529**, 221–225 (2016).
3. Gerbe, F. et al. Intestinal epithelial tuft cells initiate type 2 mucosal immunity to helminth parasites. *Nature* **529**, 226–230 (2016).
4. Howitt, M. R. et al. Tuft cells, taste-chemosensory cells, orchestrate parasite type 2 immunity in the gut. *Science* **351**, 1329–1333 (2016).
5. Barker, N. et al. Identification of stem cells in small intestine and colon by marker gene Lgr5. *Nature* **449**, 1003–1007 (2007).
6. Nadjsombati, M. S. et al. Detection of succinate by intestinal tuft cells triggers a type 2 innate immune circuit. *Immunity* **49**, 33–41 e37 (2018).
7. Schneider, C. et al. A metabolite-triggered tuft cell-ILC2 circuit drives small intestinal remodeling. *Cell* **174**, 271–284 e214 (2018).
8. Xiong, Z. et al. Intestinal Tuft-2 cells exert antimicrobial immunity via sensing bacterial metabolite *N*-undecanoylglycine. *Immunity* **55**, 686–700 e687 (2022).
9. McGinty, J. W. et al. Tuft-cell-derived leukotrienes drive rapid anti-helminth immunity in the small intestine but are dispensable for anti-protist immunity. *Immunity* **52**, 528–541 e527 (2020).
10. van Es, J. H. et al. Dll1+ secretory progenitor cells revert to stem cells upon crypt damage. *Nat. Cell Biol.* **14**, 1099–1104 (2012).
11. Buczacki, S. J. et al. Intestinal label-retaining cells are secretory precursors expressing Lgr5. *Nature* **495**, 65–69 (2013).
12. Yan, K. S. et al. Intestinal enteroendocrine lineage cells possess homeostatic and injury-inducible stem cell activity. *Cell Stem Cell* **21**, 78–90 e76 (2017).
13. Higa, T. et al. Spatiotemporal reprogramming of differentiated cells underlies regeneration and neoplasia in the intestinal epithelium. *Nat. Commun.* **13**, 1500 (2022).
14. Tetteh, P. W. et al. Replacement of lost Lgr5-positive stem cells through plasticity of their enterocyte-lineage daughters. *Cell Stem Cell* **18**, 203–213 (2016).
15. Barriga, F. M. et al. Mex3a marks a slowly dividing subpopulation of Lgr5⁺ intestinal stem cells. *Cell Stem Cell* **20**, 801–816 e807 (2017).
16. Nusse, Y. M. et al. Parasitic helminths induce fetal-like reversion in the intestinal stem cell niche. *Nature* **559**, 109–113 (2018).
17. Yui, S. et al. YAP/TAZ-dependent reprogramming of colonic epithelium links ECM remodeling to tissue regeneration. *Cell Stem Cell* **22**, 35–49 e37 (2018).
18. Elmentaite, R. et al. Cells of the human intestinal tract mapped across space and time. *Nature* **597**, 250–255 (2021).
19. Esmaeilniakooshkghazi, A., George, S. P., Biswas, R. & Khurana, S. Mouse intestinal tuft cells express advillin but not villin. *Sci Rep.* **10**, 8877 (2020).
20. Ruppert, A. L. et al. Advillin is a tuft cell marker in the mouse alimentary tract. *J. Mol. Histol.* **51**, 421–435 (2020).
21. Artegiani, B. et al. Fast and efficient generation of knock-in human organoids using homology-independent CRISPR–Cas9 precision genome editing. *Nat. Cell Biol.* **22**, 321–331 (2020).
22. Hoover, B. et al. The intestinal tuft cell nanostructure in 3D. *Sci. Rep.* **7**, 1652 (2017).
23. Beumer, J. & Clevers, H. Cell fate specification and differentiation in the adult mammalian intestine. *Nat. Rev. Mol. Cell Biol.* **22**, 39–53 (2021).
24. Sakaue-Sawano, A. et al. Visualizing spatiotemporal dynamics of multicellular cell-cycle progression. *Cell* **132**, 487–498 (2008).
25. Smillie, C. S. et al. Intra- and inter-cellular rewiring of the human colon during ulcerative colitis. *Cell* **178**, 714–730 e722 (2019).
26. Baran, Y. et al. MetaCell: analysis of single-cell RNA-seq data using K-nn graph partitions. *Genome Biol.* **20**, 206 (2019).
27. Hickey, J. W. et al. Organization of the human intestine at single-cell resolution. *Nature* **619**, 572–584 (2023).
28. Geurts, M. H. et al. CRISPR-based adenine editors correct nonsense mutations in a cystic fibrosis organoid biobank. *Cell Stem Cell* **26**, 503–510 e507 (2020).
29. de Lau, W. et al. Peyer's patch M cells derived from Lgr5(⁺) stem cells require SpiB and are induced by RankL in cultured "miniguts". *Mol. Cell. Biol.* **32**, 3639–3647 (2012).
30. Bjerknes, M. et al. Origin of the brush cell lineage in the mouse intestinal epithelium. *Dev. Biol.* **362**, 194–218 (2012).
31. Beumer, J. et al. High-resolution mRNA and secretome atlas of human enteroendocrine. *Cell* **181**, 1291–1306 e1219 (2020).
32. van der Flier, L. G. et al. Transcription factor achaete scute-like 2 controls intestinal stem cell fate. *Cell* **136**, 903–912 (2009).
33. Bosurgi, L. et al. Macrophage function in tissue repair and remodeling requires IL-4 or IL-13 with apoptotic cells. *Science* **356**, 1072–1076 (2017).
34. Ayyaz, A. et al. Single-cell transcriptomes of the regenerating intestine reveal a revival stem cell. *Nature* **569**, 121–125 (2019).
35. May, R. et al. Brief report: Dclk1 deletion in tuft cells results in impaired epithelial repair after radiation injury. *Stem Cells* **32**, 822–827 (2014).
36. Nakanishi, Y. et al. Dclk1 distinguishes between tumor and normal stem cells in the intestine. *Nat. Genet.* **45**, 98–103 (2013).
37. Westphalen, C. B. et al. Long-lived intestinal tuft cells serve as colon cancer-initiating cells. *J. Clin. Invest.* **124**, 1283–1295 (2014).
38. Billipp, T. E., Nadjsombati, M. S. & von Moltke, J. Tuning tuft cells: new ligands and effector functions reveal tissue-specific function. *Curr. Opin. Immunol.* **68**, 98–106 (2021).

Article

Methods

Fetal and adult tissues

Uninflamed ileum, duodenum and colon were obtained from patients undergoing tumour-resection surgery; tissues were collected at an appropriate distance from the tumour. The resection specimen was obtained as residual material after clinical procedures in accordance with the Declaration of Helsinki, the ethical guidelines of the University Medical Centre Utrecht, Utrecht, and Amsterdam University Medical Centre, Amsterdam, the Netherlands. All adult tissue material used in this study was obtained after informed consent, and with approval of tissue-specific protocols by the Medical Ethical Committee of the respective University Medical Centers.

Human fetal tissue was obtained from elective abortions at the Stichting Bloemenhove clinic in Heemstede, the Netherlands, on on the receipt of informed consent. The use of human abortion tissues was approved by the Medical Ethical Committee of the Academic Medical Center, Amsterdam, the Netherlands. Gestational age, determined by ultrasonic measurement of the diameter of the skull or femur, ranged from 19 to 21 weeks.

Generation and culturing human intestinal organoids

Human intestinal cells were isolated, processed and cultured as previously described[39,40]. Organoids were routinely tested for mycoplasma contamination and resulted negative. The details of organoid donors used in each experiment are listed in Supplementary Table 1.

Human intestinal organoids were split once a week by mechanic dissociation. In this study, basic culture medium includes advanced Dulbecco's modified Eagle's medium/F12 (Gibco) supplemented with 100 U ml^{-1} penicillin–streptomycin (Gibco), 10 mM HEPES (Gibco), 1× Glutamax (Gibco), 1× B-27 Supplement (Life Technologies), 1.25 mM N-acetylcysteine (Sigma-Aldrich) and 1% (v/v) recombinant Noggin (U-Protein Express).

Organoids were expanded in human expansion medium as previously described[39]. For differentiation towards tuft cells, organoids were washed 30 min in DMEM+++ at day 4 and the medium was replaced for tuft cell differentiation medium (diff): 0.5 nM Wnt surrogate (U-Protein Express), 20% (v/v) R-spondin1 (conditioned medium), 50 ng ml^{-1} recombinant human EGF (Peprotech), 10 μM Notch inhibitor DAPT (Sigma-Aldrich) in basic culture medium. For tuft cell differentiation with IL-4 and IL-13, EGF was withdrawn, 5 ng ml^{-1} human IL-4 (Peprotech) and 5 ng ml^{-1} human IL-13 (Peprotech) were supplemented to tuft cell differentiation medium. BMP activation was achieved by withdrawing Noggin and addition of 50 ng ml^{-1} BMP2 (Peprotech) and 50 ng ml^{-1} BMP4 (Peprotech). Mature enterocytes and Paneth cell differentiation was achieved by using EGF, R-spondin1, BMP2/4 (ERB medium)[41] or 10 ng ml^{-1} human IL-22 (Peprotech) in WENRA[42] (Wnt/R-spondin1, EGF, Noggin, ALK4,5,7 inhibitor (A83-01, Tocris)) medium, respectively. For specific experiments, 10 ng ml^{-1} human IL-27 (Peprotech), 10 ng ml^{-1} human IL-25 (Peprotech), 10 ng ml^{-1} human SCF (Peprotech), 50 ng ml^{-1} recombinant human Epiregulin (Peprotech), were used.

For organoid outgrowth experiments (Fig. 3a and Extended Data Fig. 6a–d), 100 single cells per 10 μl of basement membrane extract (BME) were seeded, and replated at day 3, keeping similar seeding density between tuft cell and non-tuft cell conditions.

For irradiation experiments, culture plates were sealed air-tight and irradiated with a single fraction of 5–6 Gy (Fig. 4c and Extended Data Fig. 8j–k) using a linear accelerator (Elekta Precise Linear Accelerator 11F49, Elekta). The plates were positioned on top of 2 cm-thick polystyrene and submerged in a 37 °C water bath and radiated from below with the plate being positioned at exactly 100 cm from the radiation source.

For irradiation of AVIL lineage tracing organoids (Fig. 4g–i), organoids were differentiated for 4 days in tuft cell differentiation medium with IL-4 and IL-13, exposed to 1 μM Tamoxifen for 20 h, then the organoids were split and irradiated (9 Gy) 1 day after splitting.

Generation of stable genetically modified organoids

For reporters, for generation reporter organoids using a CRISPR–HOT approach as described in ref. 21, human duodenum, ileum and colon organoids were dissociated into small clumps, washed twice with Opti-MEM (Thermo Fisher scientific) and resuspended in BTXpress solution (BTX). Clumps were resuspended with a targeting plasmid containing a fluorescent protein (Clover, mNeon or tdTomato), which can be linearized at a defined base position by a specific single-guide RNA (sgRNA) and Cas9 (provided from a second plasmid, frame selector plasmid that also encodes mCherry). These two plasmids were co-electroporated with a plasmid encoding the sgRNA for the gene locus (Supplementary Table 2, Addgene nos. 47108, 66939, 66940, 138569, 174092). Following blasticidin selection or cell sorting based on mCherry signal, clones were picked and successful incorporation was confirmed by Sanger sequencing (Macrogen).

Regarding knock-outs, for generation knock-out organoid lines using base-editing or conventional CRISPR–Cas9, spacer sequences for sgRNAs were cloned as previously described in the empty sgRNA backbone that was a kind gift from K. Joung (BPK1520, Addgene no. 65777)[28]. In short, plasmids were amplified using -inverse PCR (Q5, NEB), using primers with overhangs containing spacer sequences. PCR amplicons were subsequently ligated using T4 ligase (NEB) in a reaction with DpnI (NEB) to remove PCR template material. Ligations were transformed into MACH1T1 cells (Thermo Fisher) and sgRNA identity was confirmed by Sanger sequencing. For electroporation, 2.5 μg sgRNA plasmid (BPK1520, Addgene no. 65777), 7.5 μg pCMV_AncBE4max_P2A_GFP plasmid (for base-editing, Addgene no. 112100) or pCAS9-mCherry-Frame +1 plasmid (for conventional CRISPR–Cas9, Addgene no. 66940), together with 10 μg PiggyBac transposon system (5 μg transposase + 5 μg hygromycin resistance containing transposon)[43] were co-electroporated into human duodenum, ileum and colon AVIL-Clover reporter organoids. The ATOH1$^{-/-}$ line was generated in human ileum wild-type organoids. After hygromycin selection, subclones were genotyped. Knock-out clones were further expanded for the following experiments. The list of guide RNAs (gRNAs) and primers to genotype can be found in Supplementary Table 2.

For FUCCI and overexpression constructs, for generation of the FUCCI reporter, ATOH1 overexpression and H2B-iRFP in human ileum AVIL-Clover reporter organoids using transposon system, constructs were cloned into a p2T-based vector[44] using Gibson Assembly (NEBuilder HiFi DNA Assembly). The FUCCI sequence comprising mCherry-Cdt1-T2A-Geminin-hmAzami-Green was PCR-amplified from a construct provided as a kind gift by G. Kops (Hubrecht institute, Utrecht). The ATOH1-P2A-iRFP670 overexpression plasmid was cloned using a three-insert Gibson reaction. ATOH1 complementary DNA (IDT) was first cloned into a backbone vector with GSlinker-P2A-iRFP670, and the complete fragment of ATOH1-GSlinker-P2A-iRFP670-SV40polyA was amplified. The DNA fragment of tight TRE promoter with the ATG start codon and 3XFLAG tag was amplified from pCW-Cas9 (Addgene no. 50661). The DNA fragment of hPGK-PuroR-rTetR was amplified from pCW-Cas9. All three DNA fragments were then cloned in the digested backbone. For continuous expression H2B-iRFP670, the H2B-iRFP670 and IRES-Puromycin sequences were PCR-amplified, respectively, then were inserted into the p2T vector cut with NheI (Promega) and SmaI (Promega). Organoid lines were generated by co-electroporation of 5 μg of the respective FUCCI, ATOH1-P2A-iRFP670 or H2B-iRFP670 expression construct together with 5 μg of mT2TP transposase mediating the tol2-dependent random integration of the expression constructs into the cell genome.

For generation POU2F3 overexpression in human duodenum, colon organoids using lentivirus system, a gBlock for POU2F3 was ordered from IDT, which contained a 5′ untranslated region sequence, including an EcoRI site and a Kozak sequence, and 3′ tag sequence instead of the STOP codon, which includes a Gly linker, HA tag, P2A

sequence and another EcoRI site. This gBlock was cloned into a pJet vector and an EcoRI restriction enzyme cloning step was done to introduce the *POU2F3* sequence into pLX vector, which enable the doxycycline-induced *POU2F3*-P2A-tdTomato expression[31]. Organoids were lentivirally transduced as previously described[45].

For lineage tracing, human ileum organoids were targeted with a tdTomato and CreERT2 sequence fused with the gene encoding for Advillin using a CRISPR–HOT approach as described in ref. 21 (tdTomato-T2A-CreERT2 to the *AVIL* locus separated by a P2A sequence to obtain AVIL-P2A-tdTomato-T2A-CreERT2). In parallel, using mT2TP transposase-based random integration, a CAG promoter-driven loxp-flanked puromycin resistance containing a stop codon with a downstream H2B-iRFP670 was introduced (CAG-loxp-puromycin-stop-loxp-H2B-iRFP670).

Transmission electron microscopy
Organoids were chemically fixed for 3 h at room temperature with 1.5% glutaraldehyde in 0.067 M cacodylate buffered to pH 7.4 and 1% sucrose. Samples were washed once with 0.1 M cacodylate (pH 7.4), 1% sucrose and three times with 0.1 M cacodylate (pH 7.4), followed by incubation in 1% osmium tetroxide and 1.5% K4Fe(CN)6 in 0.1 M sodium cacodylate (pH 7.4) for 1 h at 4 °C. After rinsing with Milli-Q water, organoids were dehydrated at room temperature in a graded ethanol series (70, 90, up to 100%) and embedded in Epon polymerized for 48 h at 60 °C. Ultrathin sections of 60 nm were cut using a diamond knife (Diatome) on a Leica UC7 ultramicrotome, and transferred onto 50 Mesh copper grids covered with a Formvar and carbon film. Sections were poststained with uranyl acetate and lead citrate.

All transmission electron microscopy images were collected autonomously using a virtual nanoscopy slide[46] on a Tecnai T12 microscope (Thermo Fisher Scientific) at 120 kV using an Eagle camera. Data were stitched, uploaded, shared and annotated using Omero v.5.6.x and Path-Viewer v.3.7. The final pictures were directly acquired at the microscope in a manual standard way, using the Eagle camera at 4,000 × 4,000.

RNA isolation and qPCR
Organoid RNA was isolated using RNAeasy kit (Qiagen), following the manufacturer's protocol. qPCR analysis using Bio-Rad CFX Manager v.3.1 and Microsoft Excel was used to perform biological and technical replicates as previously described[47]. Primers are listed in Supplementary Table 3.

Flow cytometry
Organoids were dissociated into single cells using TrypLE (TrypLE Express, Life Technologies) with 10 μM Rho kinase inhibitor (Abmole) in 37 °C and mechanical disruption by pipetting every 5 min. Cells were stained for 30 min with antibody, then were visualized using a BD LSR Fortessa X20 4 laser (BD Biosciences, FACSDiva v.9.0) or sorted using BD FACS (fluorescence activated cell sorting) Influx (BD Biosciences, v.1.2.0.142) based on fluorescence levels. FlowJo software (v.10.6.2) was used to analyse the flow cytometry data. For scRNA-seq, single cells were sorted on FACSFusion (BD Biosciences, FACSDiva v.8.0.1) and collected in 384-well plates with ERCC spike-ins (Agilent), reverse transcription primers and deoxynucleotide triphosphates (both Promega). Single-cell sequencing was performed according to the Sort-seq method[48].

For organoids staining, PE antihuman CD117 antibody (KIT; 1:100, Biolegend, 313204) or Biotin antihuman CD117 (1:100, Biolegend, 313208) and Brilliant Violet 421 Streptavidin (1:1,000, Biolegend, 405226), LIVE/DEAD Fixable Far Red Dead Cell Stain Kit (1:1,000, Thermo Fisher, L34974) were used in some experiments. For sorting from primary human fetal and adult intestine tissue, Alexa Fluor 488 antihuman CD326 (Epcam; 1:100, Biolegend, 324210), APC/Cy7 antihuman CD45 (1:100, Biolegend, 304014), PE antihuman CD117 antibody (KIT; 1:100, Biolegend, 313204) were used. For cell multiplexing oligo labelling,

organoids were digested into single cells using TrypLE (Thermo Fisher), washed three times with ice-cold PBS + 10% FBS and incubated 15 min at room temperature with 100 μl Cell Multiplexing Oligo. After washing, 8,000 live cells (4′,6-diamidino-2-phenylindole negative (DAPI⁻) cells) per condition were sorted into collection tube, were subjected to droplet-based scRNA-seq using the 10X Genomics platform.

Histology and immunostainings
For immunostainings, sections of formalin-fixed, paraffin embedded human colon and ileum tissue were obtained from resections performed at the University Medical Center Utrecht, the Netherlands. Anonymized archival pathology material was used according to the guidelines of the University Medical Center Utrecht's Research Ethics Committee[49]. The human intestine tissues were fixed for 2 h at room temperature in 4% formalin, embedded in paraffin and stained as described previously[50]. Rabbit anti-Advillin (1:500, Sigma-Aldrich, HPA058864), mouse anti-Ki67 (1:4,000, monosan, MONX10283), rabbit antichromogranin A (1:600, labned.com, LN1401487) followed by goat antirabbit (ready to use, Immunologic, DPVR110HRP) or EnVision kits antimouse (ready to use, Dako, K4001) conjugated to horseradish peroxidase and then visualized (VS200 slide scanner, software v.VS200 ASW 3.3, Olympus-Lifescience).

Whole-mount staining of organoids was performed as previously described[51]. In brief, organoids were removed from the BME, then were fixed 2 h at room temperature in formalin. Next, the organoids were permeabilized using 0.1% Tween 20 (Sigma-Aldrich) in PBS for at least 15 min and blocked for at least 1 h in 0.1% Triton X-100 (Sigma-Aldrich), 1 g l⁻¹ bovine serum albumin (Sigma-Aldrich) in PBS. Primary antibodies used were rabbit anti-AVIL (1:300, Sigma-Aldrich, HPA058864), rabbit anti-POU2F3 (1:100, Sigma-Aldrich, HPA019652), goat anti-GFP (1:600, Abcam, ab6673), mouse anti-Ki67 (1:100, BD Pharminge, 550609), rabbit antichromogranin A (1:100, labned.com, LN1401487), rabbit antimucin 2 (1:200, Santa Cruz Biotechnology, sc-15334), rabbit anti-APOB (1:100, Novus Biologicals, NBP2-38608), rabbit anti-Lysozyme antibody (1:100, GeneTex, GTX72913), rabbit anti-Vimentin (1:100, Cell Signaling technology, 5741S), mouse anti-TM4SF4 antibody (1:100, Sigma-Aldrich, sc-293348), APC Mouse antihuman CD274 (1:100, BD Pharmingen, 563741), goat anti-GNAT3 (1:100 in organoids, LSBio, LS-B4942), goat anti-GNAT3 (1:500 in human intestine tissue slides, OAEB00418, Aviva Systems Biology), rabbit anti-CD117 (c-kit, 1:100, DAKO, A4502). Organoids were incubated with Alexa Fluor 488 phalloidin (1:1,000, Thermo Fisher Scientific, A12379) or phalloidin-atto647N (1:1,000, Sigma-Aldrich, 65906), with the corresponding secondary antibodies Alexa Fluor 405 donkey antirabbit (1:1,000, Thermo Fisher Scientific, A48258), Alexa Fluor 488 donkey antimouse (1:1,000, Thermo Fisher Scientific, A21202), Alexa Fluor 488 donkey antigoat (1:1,000, Thermo Fisher Scientific, A11055), Alexa Fluor 568 donkey antirabbit (1:1,000, Thermo Fisher Scientific A10042), Alexa Fluor 647 goat antimouse (1:1,000, Thermo Fisher Scientific, A21236), Alexa Fluor 647 donkey antirabbit (1:1,000, Thermo Fisher Scientific, A31573) and DyLight 755 donkey antirabbit (1:1,000, Molecular Probes, Thermo Fisher Scientific, SA5-10043) in blocking buffer containing DAPI (1:1,000, Invitrogen, D1306). Sections were embedded in fructose–glycerol clearing solution, then visualized on Leica SP8 confocal microscope (LAS X v.1.1). Image analysis was performed using ImageJ (Fiji, v.1.51n) and Imaris (Andor Technology, v.x64 9.3.1) software.

Some images were obtained using a Zeiss LSM880 confocal microscope with Airyscan (Carl Zeiss, software version ZEN 2) and a LCI Plan-Neofluar ×63 numerical aperture (NA) 1.3 water immersion objective (Carl Zeiss) at a voxel resolution of 0.04 μm (*x/y*) to 0.19 μm (*z*). Images were deconvoluted using the Zen Black (Carl Zeiss)-inbuild Airyscan postprocessing module. Images were processed (Gauss filtering) using Fiji and rendered in Imaris.

STED super resolution microscopy was performed using a Leica STELLARIS 8 STED microscope (software v.4.7.0.28176) using a HC PL

Article

APO CS2 ×100 NA 1.40 oil objective. Organoids expressing AVIL-Clover were fixed, stained with DAPI and phalloidin-atto647N and mounted on 0.16–0.19-mm-thick cover glasses (Glaswarenfabrik Karl Hecht GmbH & Co KG) in ProLong Gold Antifade Mountant (Thermo Fisher Scientific). Tuft cell reporter and DAPI signal were recorded with confocal resolution and tuft cells identified. The actin cytoskeleton was visualized with super resolution microscopy with a pixel resolution of 10 × 10 nm. To do so, phalloidin-atto647N was illuminated with 647 nm excitation and 775 depletion lasers. The signal was recorded with a line averaging of 16, a dwell time of 0.69 µs.

For clustering analysis, the surface of organoids in three-dimensional image stacks was projected into two dimensions using the LocalZProjector Fiji plugin based on DAPI-stained nuclei and tuft cells were segmented using the ITK-SNAP software (v.3.8.0). For the clustering analysis, a custom-made MATLAB script was used. Inter-tuft cell distance was measured based on the Euclidean distance of their centroid position and expressed as a multiple of the average cell distance. A density map was computed, and a contour plot was generated using the imcontour function. Clusters were identified within an eight-cell-distance and analysed using the MATLAB package 'Distance-based clustering of a set of xy coordinates' (Y. Marcon (2023), https://www.mathworks.com/matlabcentral/fileexchange/56150-distance-based-clustering-of-a-set-of-xy-coordinates), made available through the MATLAB Central File Exchange.

Live-cell imaging of human intestinal organoids

Live imaging experiments were performed on a Leica SP8 confocal laser scanning microscope equipped with Argon laser and White Light Laser at 37 °C and 5% CO_2 using a Leica ×20 NA 0.7 air objective. Images were acquired in a line-sequential mode separating the fluorophore recordings with minimal spectral overlap with a final pixel resolution of 1.65 pixels per micrometre, an axial resolution of 1.4 µm and a time interval of 9 min.

Long-term live imaging was performed using a LS1 Live light sheet microscope (Viventis Microscopy, software v.2.0.0.3) using a Nikon ×25 NA 1.1 water immersion objective at a magnification of ×18. Organoids were mounted on a single-chamber sample holder 1 day before the start of imaging. A position-specific alignment of the light sheets with a thickness of 2.2 µm was done. The samples were imaged with a 488 and 561 nm illumination to visualize Clover- and tdTomato-based reporters with a time interval of 10 min at 37 °C and 5% CO_2.

The postacquisitional analysis was done with custom-made Fiji script, the H.264 encoding was done using HandBrake (v.1.8.1) software.

scRNA-seq analysis

scRNA-seq libraries of organoid-derived material, and KIT⁺ enriched cells from fetal and adult intestines were sequenced on an Illumina NextSeq platform, at a median sequencing depth of 49,861 reads per cell. Reads were mapped to a human genome (hg38) integrated with the Clover transcript using STAR (v.2.7.8a), reads with many mapping positions were excluded. Reads were associated with genes if they were mapped to an exon. Reads were demultiplexed and collapsed into unique molecular identifier (UMI) tables using umi_tools (v.1.1.1) allowing up to one hamming distance of the cell barcode. Cells with less than 500 UMI or with more than 40% mitochondrial genes were excluded from analysis.

All analysis was performed in R. We used the MetaCell package (v.0.3.5)[26] to analyse all scRNA-seq data collected in this study. Default parameters were used unless otherwise stated. We derived a Meta-Cell cover of DAPI⁻/AVIL-Clover⁺ and DAPI⁻ epithelial cells from human ileal organoids. Mitochondrial genes and the highly variable immunoglobulin genes (IGH, IGK and IGL prefixes) were removed from the UMI tables. Gene features for MetaCell covers were selected using the parameter Tvm=0.1, total umi more than ten and more than three UMI in at least three cells. We filtered the list of gene features used for

MetaCell analysis from genes associated with cell cycle, immediate stress response and gene modules inducing strong patient-specific biases. To this end, we first identified all genes with a correlation coefficient of at least 0.13 for one of the anchor genes *TOP2A*, *MKI67*, *PCNA*, *MCM4*, *UBE2C*, *STMN1*, *FOS*, *EGR1*, *IER3*, *FOSB*, *HSPA1B*, *HSPA1A*, *HSP90AA1* and *DNAJB1*. We then hierarchically clustered the correlation matrix between these genes (filtering genes with low coverage and computing correlation using a down-sampled UMI matrix) and selected the gene clusters that contained the above anchor genes. We thus retained 94 genes as features. We used MetaCell to build a k-nearest neighbours graph, perform boot-strapped coclustering (500 iterations; resampling 70% of the cells in each iteration) and derive a cover of the coclustering k-nearest neighbours graph ($k = 30$). Outlier cells featuring a gene expression higher than fourfold than the geometric mean in the metacells in at least one gene were discarded. Detailed annotation of the different tuft and epithelial cell subsets was performed using hierarchical clustering of the MetaCell confusion matrix. ClusterProfiler[52] (v.3.14.0) and ChIPpeakAnno (v.3.20.0) were applied to perform gene functional annotation of DEGs.

scRNA-seq of passage 1 day 7 KIT⁻- and KIT⁺-derived organoids was performed using the Chromium Next GEM Single Cell 3′ v.3.1 platform, and sequenced on an Illumina NovaSeq6000 platform. Reads were mapped to the human genome (hg38) and demultiplexed using cellranger (v.7.1.0). Recovered cellplex barcodes were used to assign single cells to experimental batches. Single cells with less than 64 UMI of a specific cellplex barcodes were discarded from downstream analysis. Single cells with less than eightfold UMI count ratio between highest and second highest cellplex barcodes were marked as doublets and discarded from downstream analysis. Single cells with less than 1,000 genomic UMIs or more than 20% mitochondrial content failed to pass quality control and were discarded from further analysis, resulting in 10,311 quality control-positive cells.

Clustering of passage 1 KIT⁻- and KIT⁺-derived organoids was performed as stated above. Gene features for the MetaCell covers were selected using the parameter Tvm=0.1, total umi>15 and more than three UMI in at least three cells, resulting in 228 features.

We reanalysed scRNA-seq data from human primary intestinal tissue[18]. We selected 15,184 single cells from healthy adult small intestine, with more than 1,000 and less than 20,000 total UMI for further analysis. Cells were analysed with the MetaCell package as previously described to derive a two-dimensional (2D) representation of the data for Extended Data Figs. 3a and 5b. Otherwise, we used predefined annotations to epithelial cell types. In Extended Data Figs. 3j and 5f we sampled 500 cells from each cell types out of the total 77,364 healthy adult single cells in that database.

Quantification and statistics

No statistical methods were used to predetermine sample size. All experiments were performed in several distinct replicates, as indicated in the text and figure legends. Organoids analysed were chosen randomly. All statistical tests were two-tailed, except in Fig. 1b,d and Extended Data Fig. 1f, where different growth conditions were assessed for increased tuft cell numbers. We used Student's t-test for continuous data and Mann–Whitney test for discrete data, and used FDR adjustment to correct for many hypotheses.

Reporting summary

Further information on research design is available in the Nature Portfolio Reporting Summary linked to this article.

Data availability

Organoid and primary tissue scRNA-seq data that support the findings of this study were deposited in the Gene Expression Omnibus under accession code GSE233451, and are publicly available. To support

the main finding of this paper, we reanalysed single-cell RNA-seq data from the following sources: The Gut Cell Atlas (https://www.gutcellatlas.org/), https://doi.org/10.5061/dryad.8pk0p2ns8 (ref. 53) and Single Cell Portal: SCP259 (https://singlecell.broadinstitute.org/single_cell/study/SCP259/intra-and-inter-cellular-rewiring-of-the-human-colon-during-ulcerative-colitis). Source data are provided with this paper.

Code availability

Custom code and scripts used to analyse the data and produce the figures are available in a public GitHub repository (https://github.com/aygoldberg/TuftOrganoids/).

39. Pleguezuelos-Manzano, C. et al. Establishment and culture of human intestinal organoids derived from adult stem cells. *Curr. Protoc. Immunol.* **130**, e106 (2020).
40. Sato, T. et al. Long-term expansion of epithelial organoids from human colon, adenoma, adenocarcinoma, and Barrett's epithelium. *Gastroenterology* **141**, 1762–1772 (2011).
41. Beumer, J. et al. BMP gradient along the intestinal villus axis controls zonated enterocyte and goblet cell states. *Cell Rep.* **38**, 110438 (2022).
42. He, G. W. et al. Optimized human intestinal organoid model reveals interleukin-22-dependency of paneth cell formation. *Cell Stem Cell* **29**, 1333–1345 e1336 (2022).
43. Andersson-Rolf, A. et al. One-step generation of conditional and reversible gene knockouts. *Nat. Methods* **14**, 287–289 (2017).
44. Lin, L. et al. Comprehensive mapping of key regulatory networks that drive oncogene expression. *Cell Rep.* **33**, 108426 (2020).
45. Koo, B. K. et al. Controlled gene expression in primary Lgr5 organoid cultures. *Nat. Methods* **9**, 81–83 (2011).
46. Faas, F. G. et al. Virtual nanoscopy: generation of ultra-large high resolution electron microscopy maps. *J. Cell Biol.* **198**, 457–469 (2012).
47. Munoz, J. et al. The Lgr5 intestinal stem cell signature: robust expression of proposed quiescent '+4' cell markers. *EMBO J.* **31**, 3079–3091 (2012).
48. Muraro, M. J. et al. A single-cell transcriptome atlas of the human pancreas. *Cell Syst.* **3**, 385–394 e383 (2016).
49. Coebergh, J. W., van Veen, E. B., Vandenbroucke, J. P., van Diest, P. & Oosterhuis, W. One-time general consent for research on biological samples: opt out system for patients is optimal and endorsed in many countries. *Brit. Med. J.* **332**, 665 (2006).
50. Farin, H. F. et al. Visualization of a short-range Wnt gradient in the intestinal stem-cell niche. *Nature* **530**, 340–343 (2016).
51. Dekkers, J. F. et al. High-resolution 3D imaging of fixed and cleared organoids. *Nat. Protoc.* **14**, 1756–1771 (2019).
52. Yu, G., Wang, L. G., Han, Y. & He, Q. Y. clusterProfiler: an R package for comparing biological themes among gene clusters. *OMICS* **16**, 284–287 (2012).
53. Becker, W. Organization of the human Intestine at single cell resolution. Dryad https://doi.org/10.5061/dryad.8pk0p2ns8 (2023).

Author contributions L.H. designed and performed experiments, and interpreted results. J.H.B. conceptualized and supervised the project, designed and performed experiments, interpreted the results and wrote the paper. A.G. interpreted the results, analysed the data and wrote the paper. M.H.G. assisted with base-editing and knock-out strategies in organoid lines. D.K. performed and analysed live-cell imaging, generated and provided several constructs. G.B. generated and provided constructs. G.J.F.v.S. performed experiments and analysed single-cell data. H.B. performed immunohistochemistry experiments. L.L. provided constructs. M.Z. supervised and supported irradiation experiments. P.J.P. and C.L.-I. performed the transmission electron microscopy experiment. C.J.B. and W.A.B. provided human adult intestinal tissues. H.C. supervised the project, interpreted the results and wrote the paper.
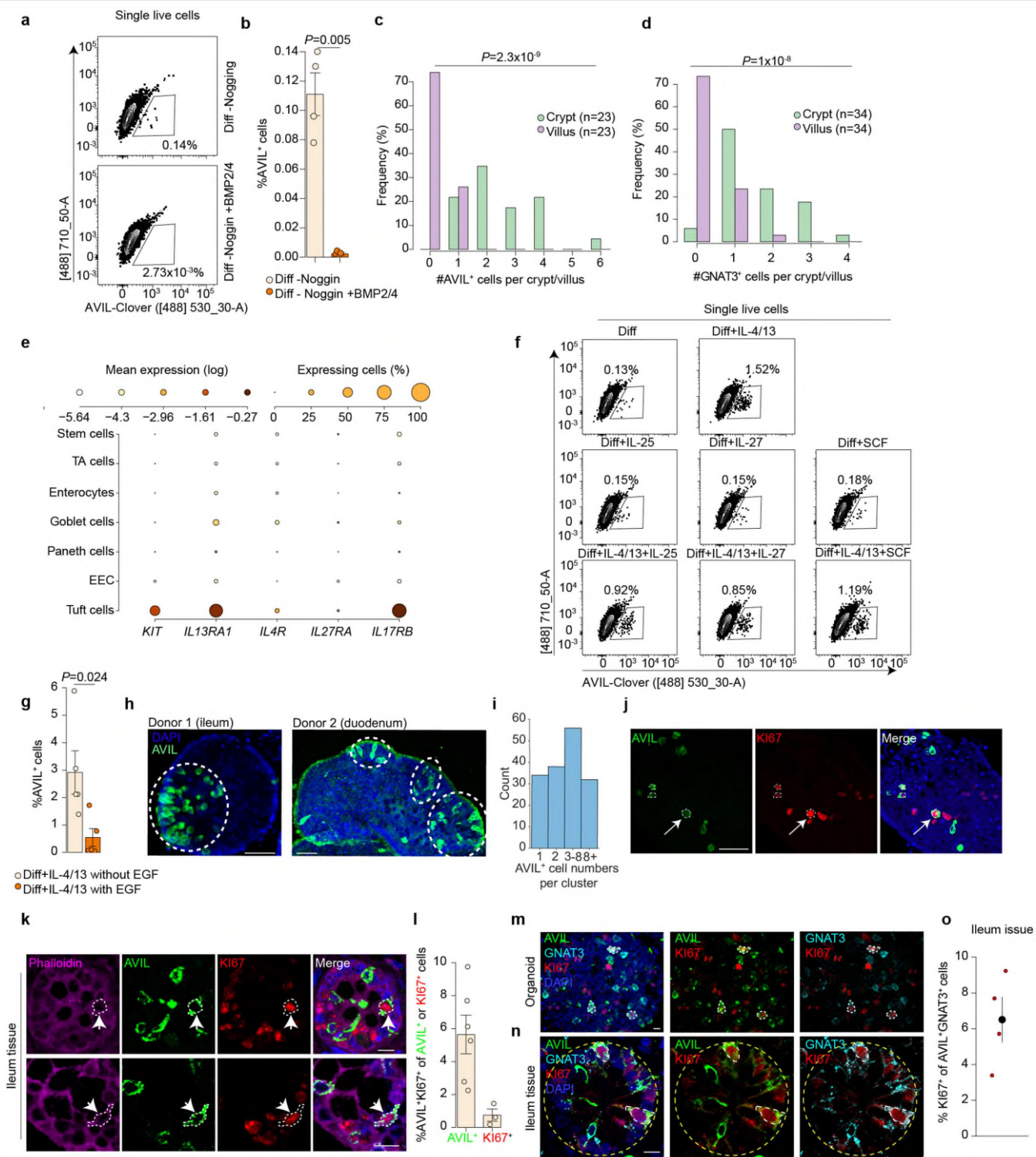
Extended Data Fig. 1 | See next page for caption.

Extended Data Fig. 1 | Flow cytometry gating strategies and quantifications of AVIL+ cells. a, Representative images of AVIL expression in human adult intestinal tissues. n = 3 donors. **b**, Schematics of generating human AVIL-Clover reporter intestinal organoids and Sanger sequencing results. n = 4 donors (Supplementary Fig. 1a). **c**, Schematics of the experimental set-up for Fig. 1b and (**d**)–(**f**). Organoids were cultured in standard human intestinal expansion medium for 4 days, then exposed to various differentiation regimens. **d**, Gating strategy for flow cytometric analysis and sorting of AVIL-Clover reporter organoids. **e**, Flow cytometric plots of the percentage of AVIL-Clover+ cells out of DAPI- cells, n = 3 independent experiments (Supplementary Fig. 1b). **f**, Quantification of DAPI- live cells in ileum organoids. Each dot is a well. n = 3 wells per condition. Results are representative of 3 independent experiments (Supplementary Fig. 1d). **g**, Fluorescence images of AVIL-Clover reporter activity with AVIL antibody staining. n = 4 donors with similar results. **h**, Phalloidin staining in differentiated human small intestinal AVIL-Clover organoids. 3 independent experiments were performed on 2 donors with similar results. **i**, Transmission electron microscopy of tuft cells in differentiated human small intestinal organoids. n = 2 donors (Supplementary Fig. 1e). **j**, qPCR quantification of tuft cell genes in sorted AVIL+ and AVIL- cells from differentiated AVIL-Clover reporter organoids. Each dot is one donor, n = 3 donors. **k**, *GNAT3* expression in a single-cell RNA sequencing dataset of human adult small intestinal tissue[18]. n = 15,184 single epithelial cells. **l**, Quantification of GNAT3 and AVIL co-staining in ileum and colon organoids (see Extended Data Fig. 2m for a representative image). n = 260 cells from 15 organoids derived from 2 organoid lines. **m-n**, Representative images (m) and quantification (n) of AVIL and GNAT3 co-staining in human ileum tissue. Yellow line marks one crypt-villus axis, arrows and magenta contours mark AVIL+ cells. Each dot is a donor. n = 4 donors. **a,g,h,i,m**, Scale bar 5 μm (**h-i**), 20 μm (**a,g**), 50 μm (**m**). **f,j,k,l,n**, Data are presented as mean values +/− standard error (**f,j,l,n**) or as mean values (**k**). **f,j**, *P* values are derived from one-tailed Student's t-test against the base medium (**f**) or two-tailed Student's t-test (**j**). TA cells: Transit-Amplifying Cells; EEC: Enteroendocrine cells; R1: R-spondin1 conditioned medium. Schematics in **b** were created using BioRender (J. van Es BioRender.com/h49r743; 2024).
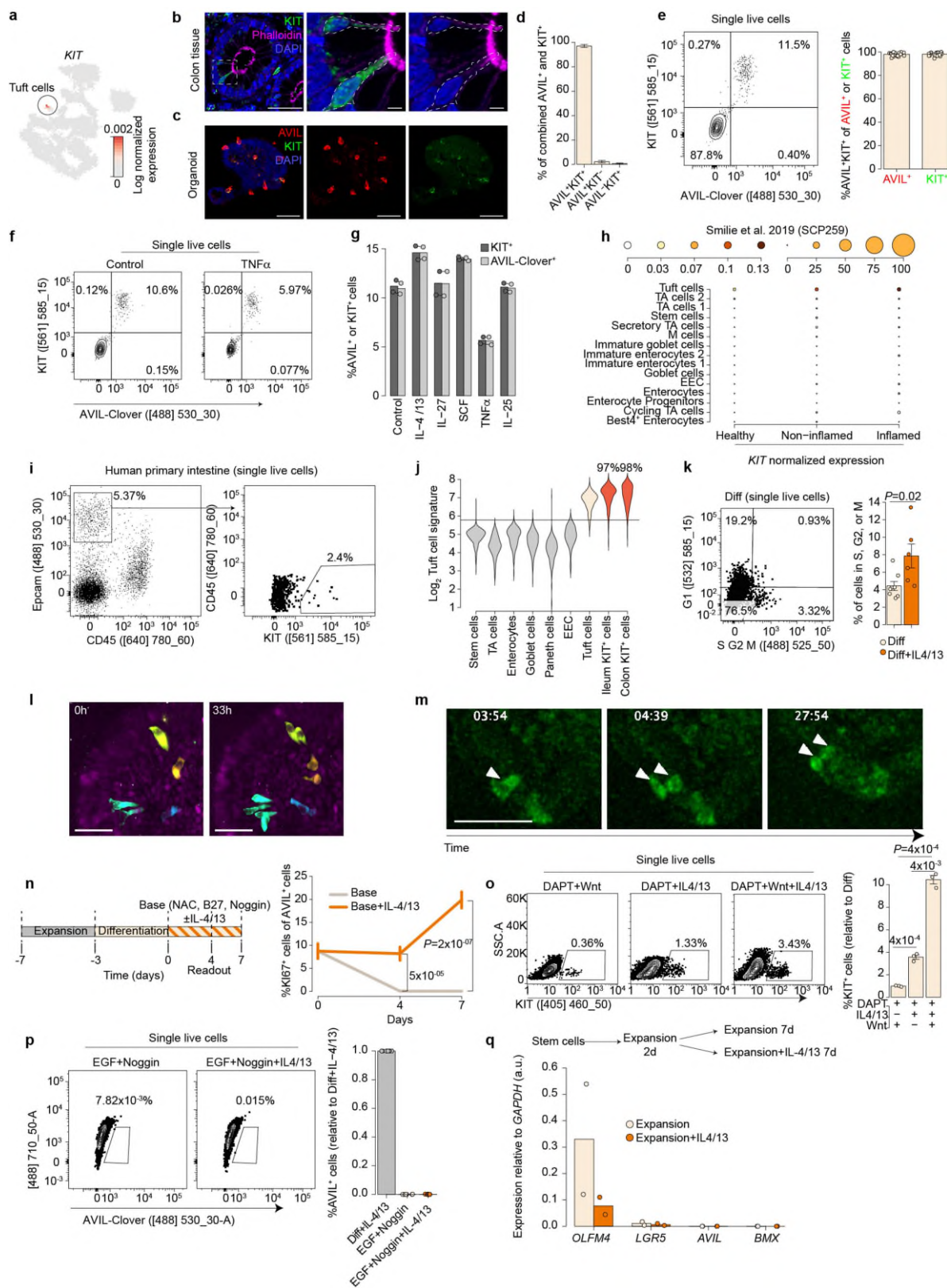
Extended Data Fig. 2 | See next page for caption.

Extended Data Fig. 2 | Tuft cell expansion in different conditions. a-b, Flow cytometric analysis (**a**) and quantification (**b**) of the percentage of AVIL^{+} cells in human ileum AVIL-Clover reporter organoids differentiated in tuft cell medium without Noggin, with or without of BMP2/BMP4. Each dot is one well. n = 4 wells per condition. Results are representative of 3 independent experiments on 2 donors (Supplementary Fig. 1f). **c-d,** Histogram of AVIL[+] (**c**) and GNAT3^{+} (**d**) cell numbers on the crypt-villus axis in human ileum tissue. n = 4 donors (Supplementary Fig. 1g). **c,** n = 23 crypt-villus axes from one donor. **d,** n = 34 crypt-villus axes pooled from four donors. **e,** Expression of selected cytokine receptors across the scRNA-seq dataset in Fig. 1a[18]. Dot color relates to size-normalized mean expression values and dot size to fraction of expressing cells. n = 15,184 single epithelial cells. **f,** Representative flow cytometric plots of AVIL-Clover reporter organoids differentiated for 4 days in tuft cell medium with indicated recombinant proteins. n = 4 donors (Supplementary Fig. 1c). **g,** Quantification of AVIL[+] cell frequency in human small intestinal AVIL-Clover organoids differentiated with IL-4/IL-13 and with or without EGF. Each dot is one well. n = 5 wells, pooled from 3 donors. **h-i,** Images (**h**) and quantification (**i**) of AVIL[+] cell clusters in IL-4 and IL-13 treated organoids. Dashed ellipses indicate clusters of AVIL^{+} cells, (Supplementary Fig. 1h). n = 988 AVIL^{+} cells (30 organoids) pooled from 2 donors. **j-k,** AVIL, KI67 co-staining in human intestine organoids (**j**) or in ileum tissues (**k**). Arrows and dashed lines indicate cells with AVIL and KI67 overlap. **j** Organoids were differentiated with IL-4/IL-13. n = 3 organoid lines derived from 2 donors (Supplementary Fig. 1i, Supplementary Video 1). **k,** n = 3 donors. **l,** Quantification of (**k**). Values indicate AVIL[+]KI67^{+} cell percentage out of the AVIL[+] or KI67^{+} cells. Each dot is a pool of at least 10 crypts, n = 1,908 cells in 323 crypts from 3 donors. **m-n,** Multiplexed staining of KI67 with AVIL and GNAT3 in organoids (**m**) and ileal tissue (**n**). Dashed white lines mark triple positive cells. **m,** n = 2 donors; **n,** Dashed yellow line demarcates a crypt. n = 4 donors. **o,** Quantification of (**n**). Each dot is a donor, n = 248 tuft cells from 4 donors. **h,j,k,m,n,** Scale bar 40 µm (**h,j**), 10 µm (**k,m,n**). **b,g,l,o,** Data are presented as mean values +/− standard error. **b-d,g,** P values are derived from two-tailed Student's t-test (**b,g**), or two-tailed Fisher's exact test (**c,d**). Diff: tuft cell differentiation medium.
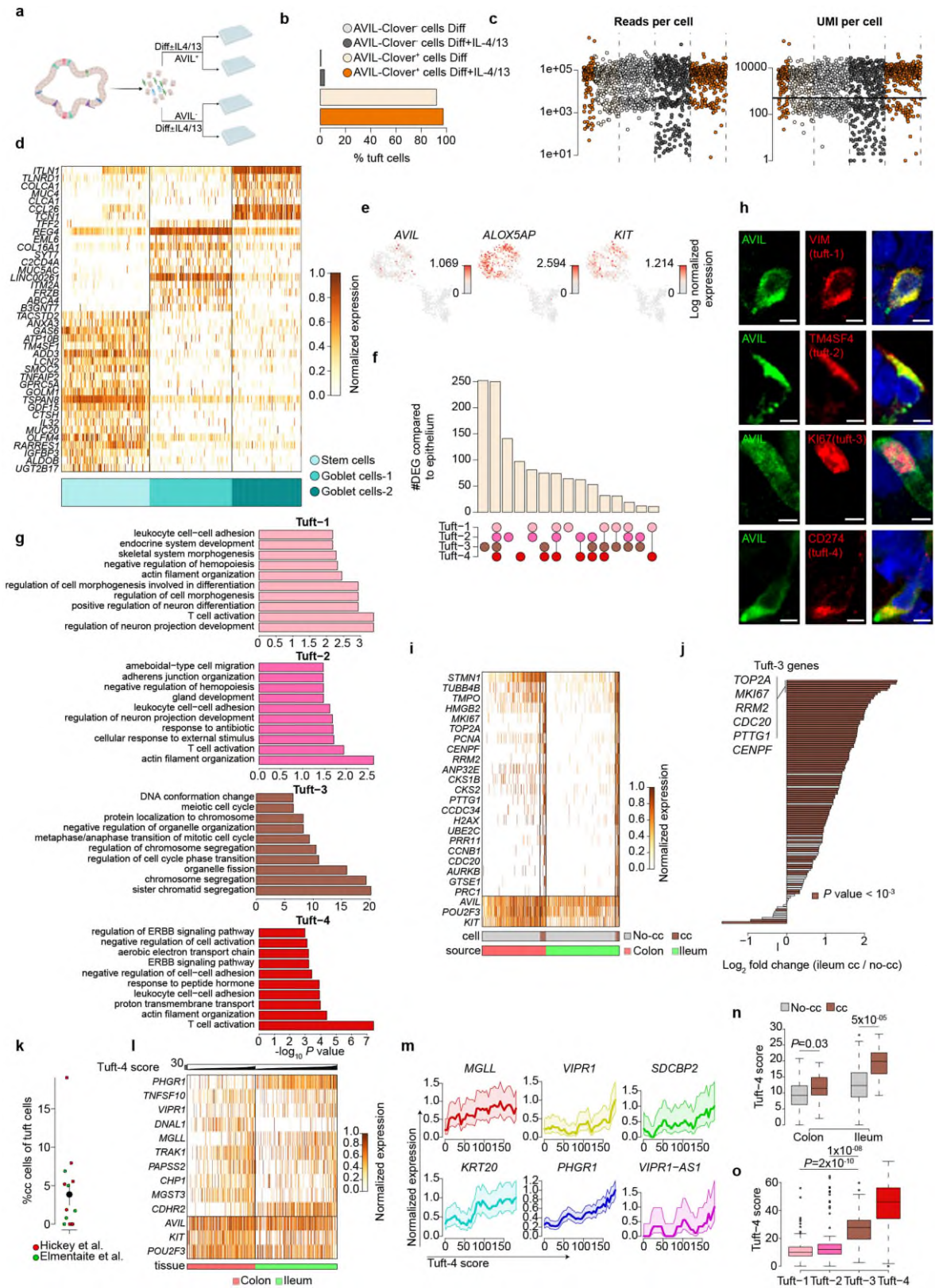
Extended Data Fig. 3 | See next page for caption.

Extended Data Fig. 3 | Proliferation dynamics of tuft cells. a, Log-normalized expression of *KIT*, projected on a Metacell 2D representation of scRNA-seq data of primary human adult small intestine[18]. n = 15,184 single epithelial cells. **b**, Co-staining of KIT and Phalloidin in human colon tissue. Two independent experiments were performed on one donor with similar results. **c-d**, Representative image (**c**) and quantification (**d**) of KIT staining in AVIL-Clover organoids. n = 303 cells of 17 organoids from 2 donors. **e**, Representative flow cytometry (left) and quantification (right) of KIT (phycoerythrin, PE) labeled AVIL-Clover organoids differentiated in tuft cell medium with IL-4/IL-13. Each dot is one well, n = 24 wells pooled from 3 donors (Supplementary Fig. 1j). **f-g**, Representative flow cytometry (**f**) and quantification (**g**) of the KIT+ and AVIL+ cells in AVIL-Clover organoids triggered with the depicted cytokines for 48 h, followed by 6 days culturing in tuft cell differentiation medium with IL-4/IL-13. Each dot is a well. n = 2 wells per condition. Results are representative of 2 donors (Supplementary Fig. 1k). **h**, *KIT* expression across epithelial cell types in healthy, IBD non-inflamed, and IBD inflamed human colon tissue[25]. Dot color relates to mean expression values and dot size to fraction of expressing cells. n = 4,428 cells. **i**, Gating strategy of sorting KIT+ cells from human primary intestine tissue. Adult colon is shown. **j**, Distribution of tuft cell gene expression signature across different epithelial populations from human adult intestine tissue[18], as well as within sorted populations of KIT+ cells from primary adult ileum and colon. Horizontal line indicates an optimal separation based on the unenriched intestine dataset. Percentage of classified tuft cells in KIT+ populations is indicated. The tuft cell signature is based on 222 core tuft cell genes shown in Fig. 2c. n = 311 ileal KIT+ cells, and 271 colon KIT+ cells. **k**, Representative flow cytometric analysis (left) and quantification (right) of the S/G2/M phase in KIT+ cells in FUCCI reporter organoids differentiated for 3 days in the indicated media. Each dot is one well. n = 8 (Diff) or 6 (Diff+IL-4/13) wells from 6 or 4 independent experiments. **l-m**, Snapshots of dividing AVIL+ cells by live-cell imaging in AVIL-Clover reporter organoids differentiated in tuft cell medium. **l**, Each dividing AVIL+ cell and its progeny are colored, 3 independent experiments were performed on 2 donors with similar results (Supplementary Video 3). **m**, Shown one tuft cell dividing twice within 24 h, 2 donors were examined with similar results (Supplementary Videos 4-5). **n**, Experimental design (left) and quantification (right) of the KI67+AVIL+ cells percentage at indicated time points., n = 800 (day 0), 631 (day 4, Base), 776 (day 4, Base+IL-4/13), 806 (day 7, Base+IL-4/13) AVIL+ cells. Results are pooled from 3 independent experiments on two organoid lines (Supplementary Fig. 1l). **o**, Representative flow cytometric analysis (left) and relative quantification (right) of KIT+ cells differentiated for 3 days in different regimens. Each dot is one well. n = 3 wells per condition, pooled from two experiments on FUCCI line (Supplementary Fig. 1m). **p**, Representative flow cytometric analysis (left) and quantification (right) of AVIL+ cell frequency in organoids differentiated for 2 days in EGF Noggin medium (without Wnt, R-spondin1 and DAPT), followed by 4 days culturing in indicated media. Each dot is a well, n = 7 wells per condition, pooled from 3 independent experiments on two lines from one donor. **q**, Experimental design (top) and qPCR quantification (bottom) of tuft cell and stem cell genes in sorted single cells from organoids cultured in human expansion medium. Each dot is a donor, n = 2 donors. **b,c,l,m**, Scale bar, 50 μm. **d,e,g,k,n-q**, Data are presented as mean values +/− standard error (**d,e,k,n-p**) or as mean values (**g,q**). **k,n,o**, *P* values are derived from two-tailed t-test. TA cells: Transit-Amplifying Cells; EEC: Enteroendocrine cells; Diff: tuft cell differentiation medium.
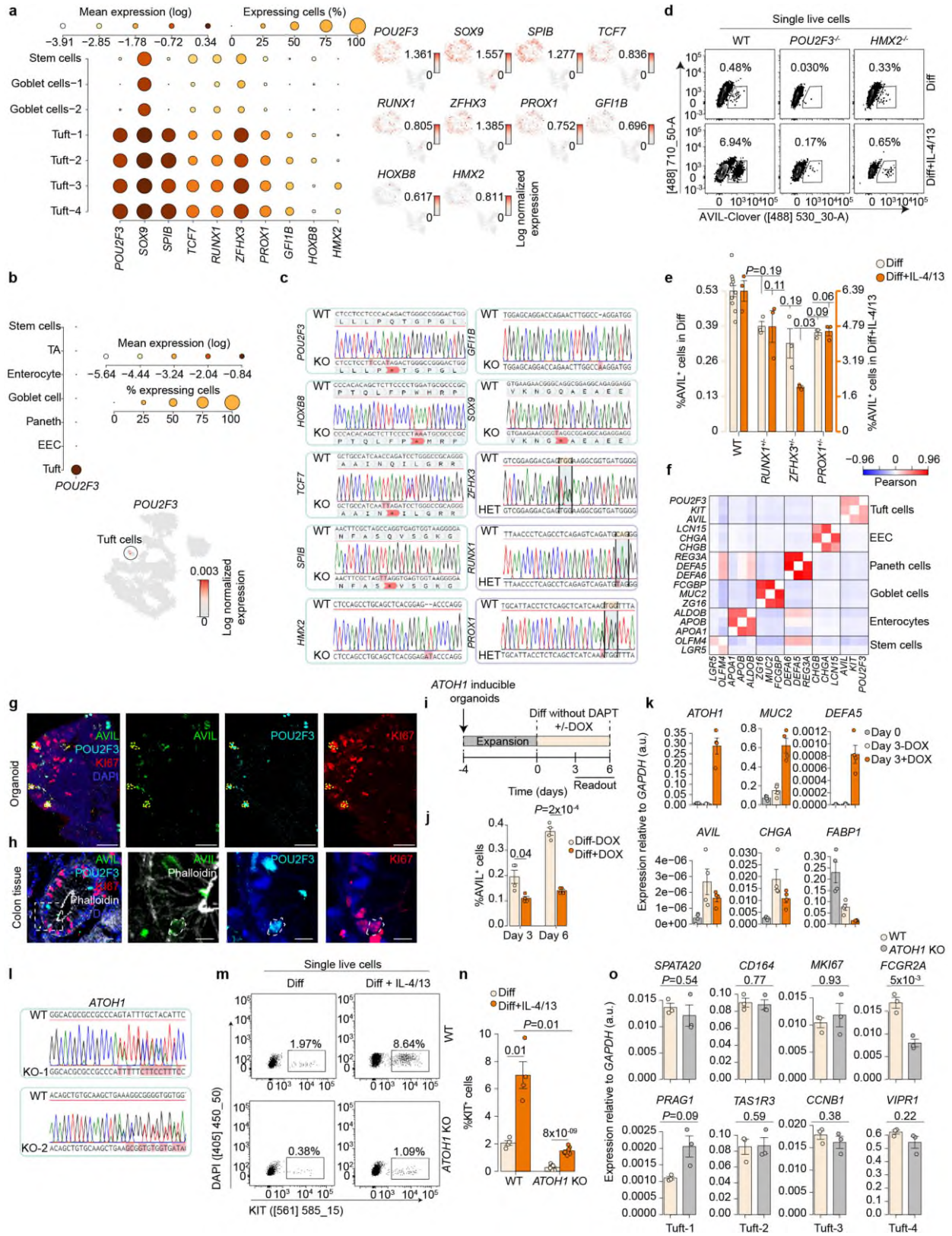
Extended Data Fig. 4 | See next page for caption.

Extended Data Fig. 4 | Analysis of single cell RNA sequence used in this study. a, Schematic overview of the scRNA-seq experiment. **b**, Tuft cell frequency in different medium and gating combinations, as determined by scRNA-seq analysis. **c**, scRNA-seq statistics, depicting number of reads per cell (top) and number of unique molecular identifiers (UMI) per cell (bottom). Each dot is a cell, colored by its gating and medium conditions. Quality threshold of 500 UMI per cell is indicated by a horizontal line. **d**, Gene expression profiles of stem cell and goblet cells. n = 373 single non-tuft cells. **e**, Expression of tuft cell marker genes projected on the metacell 2D layout as in Fig. 2a,b. Dot color indicate log normalized expression. n = 953 single cells. **f**, Summary of number of up-regulated differentially expressed genes (DEG) across the tuft-1-4 states, when compared to non-tuft epithelium. **g**, Top 10 Gene ontology terms enriched in DEG of tuft-1-4, when compared to the non-tuft cells as in (**f**). Values represent -$\log_{10}P$ value. **h**, Staining of tuft-1-4 specific markers (red, as indicated) in human ileum AVIL-reporter organoids cultured in tuft cell differentiation medium (tuft 1-2) or supplemented with IL-4/IL-13 (tuft 3-4). n = 2 independent experiments on one donor with similar results. Scale bar, 5 μm. **i**, Gene expression profiles of primary KIT+ tuft cells from human ileum and colon tissue. Shown are tuft-3 genes, as well as *KIT, POU2F3* and *AVIL*. Cells are colored by their tissue origin, and by classification into cycling cells (cc) or non-cycling cells (no-cc). n = 271 single colon and 311 single ileum KIT+ cells. **j**, Differential expression of all tuft-3 genes between 311 primary ileal cycling and non-cycling KIT+ cells as in **i**. Genes with significant differential expression (c2 test; FDR-adjusted *P* value < 10^{-3}) are colored. **k**, Estimation of the fraction of proliferating tuft cells across human primary intestine tissues from two published scRNA-seq datasets[18,27]. Each dot is a donor, n = 1,240 single tuft cells from 14 human donor samples. Data are presented as mean values +/− standard error. **l**, Gene expression profiles of 541 primary KIT+ non-cycling (no-cc) tuft cells as in **i**. Shown are tuft-4 genes, as well as *KIT, POU2F3* and *AVIL*. Cells are ordered by their expression of the aggregated tuft-4 program (top panel), and colored by their tissue origin. **m**, Expression patterns of six genes along the tuft-4 activation gradient in 213 KIT+ no-cc ileal cells. Shadings indicate 95% confidence in binomial estimation of the mean. Data was down-sampled to 1,000 UMI per cell. **n**, Aggregate expression of the tuft-4 program in cycling and non-cycling cells in colon and ileum. n = 582 single cells. **o**, Aggregate expression of the tuft-4 program across tuft cell substates in organoids as in Fig. 2e. n = 573 single tuft cells from organoids. **n-o**, Boxplots show data from the 25th–75th percentile and whiskers extending to the minimum and maximum within 1.5 × inter-quartile range, with dots marking outliers. *P* values are derived from two tailed Mann-Whitney test. Diff: tuft cell differentiation medium; cc: cell cycle. Schematic in **a** was created using BioRender (J. van Es BioRender.com/k22v672; 2024).
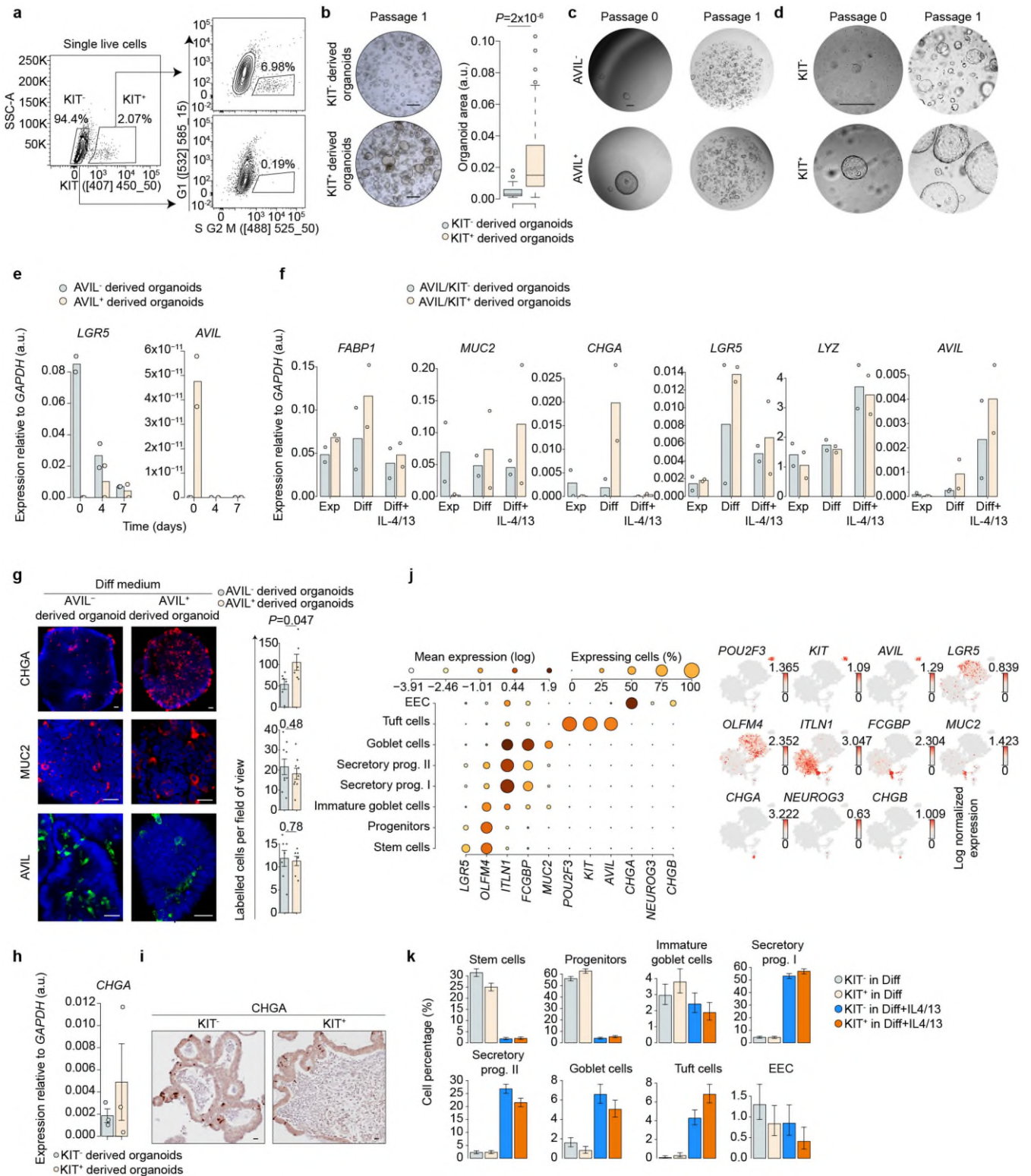
Extended Data Fig. 5 | See next page for caption.

Extended Data Fig. 5 | Transcription factor knock outs and overexpression in human ileum organoids. a-b, Expression of selected genes encoding for transcription factors across the scRNA-seq dataset from organoids as in Fig. 2a (**a**), or from human healthy adult intestine tissue[18] (**b**). Dot color relates to mean expression values and dot size to fraction of expressing cells. n = 953 cells (**a**) or n = 15,184 single epithelial cells (**b**). **c**, Genotypes of clonal transcriptional factor knock outs generated from human ileum AVIL-Clover reporter organoids. Homozygous knock outs of *POU2F3*, *HOXB8*, *TCF7*, *SPIB*, *SOX9* and heterozygous knock outs of *ZFHX3*, *RUNX1*, *PROX1* were generated using base editing (C to T) technology to induce stop codon (TAG, TAA) within exons. *HMX2*^{−/−} and *GFI1B*^{−/−} lines were generated by using conventional *CRISPR*-Cas9 method to induce frameshift. **d**, Representative flow cytometry quantification of AVIL[+] cell frequency in *POU2F3*^{−/−} and *HMX2*^{−/−} organoids. Results are representative of 3 independent experiments with similar results (Supplementary Fig. 2a). **e**, Quantification of AVIL-Clover[+] cell frequency in heterozygous knock out organoid lines by flow cytometry. Each dot is one well. n = 11 (WT Diff), or 3 (rest) wells. One of 3 independent experiments is shown (Supplementary Fig. 2c). WT Diff measurements are pooled from 4 experiments. **f**, Gene-pairwise Pearson correlation between markers of the main epithelial types across cells from primary intestinal tissue[18]. Data were down-sampled to 1,000 UMI per cell. **g-h**, Co-staining of AVIL with KI67 and POU2F3 in organoids (**g**) and primary colon tissue (**h**). Dashed lines mark triple positive cells. (**g**) n = 2 donors; **h**, Two independent experiments were performed on one donor with similar results; Scale bar, 50 μm (**g**), 5 μm (**h**). **i-k**, **i**, Schematics of the experimental set-up for (**j-k**). **j**, Quantification of AVIL-Clover[+] cell frequency in ATOH1-inducible organoids by flow cytometry. **k**, qPCR quantification of *ATOH1* and intestinal epithelial lineage markers expression. **j-k**, Each dot is a well. n = 4 wells per condition. One of 2 (**k**) or 3 (**j**) independent experiments with similar results are shown (Supplementary Fig. 2d,e). **l**, Genotype of clonal *ATOH1* knock outs generated from human ileum organoids. **m-n**, Representative flow cytometry plots (**m**) and quantification (**n**) of KIT[+] cell frequency in *ATOH1*^{−/−} organoids. Each dot is a well. n = 4 (WT), 8 (*ATOH1*^{−/−} Diff), 9 (*ATOH1*^{−/−} Diff+IL-4/13) wells, pooled from two *ATOH1*^{−/−} clonal lines from one donor (Supplementary Fig. 2f). **o**, qPCR quantification of tuft-1-4 characteristic genes in KIT^{+} cells sorted from WT and *ATOH1*^{−/−} organoids. Organoids were differentiated for 7 days in tuft cell differentiation medium with IL-4/IL-13. Each dot is a well. n = 3 wells pooled from two *ATOH1*^{−/−} lines. **i-o**, Organoids were differentiated without DAPT. **e,j,k,n,o**, Data are presented as mean values +/− standard error. **e,j,n,o**, P values are derived from FDR-adjusted two-tailed Student's t-test against the WT levels (**e**), or two-tailed Student's t-test (**j,n,o**). Diff: human tuft cell differentiation medium; TA: Transit-Amplifying Cells; EEC: Enteroendocrine cells; WT: wildtype.
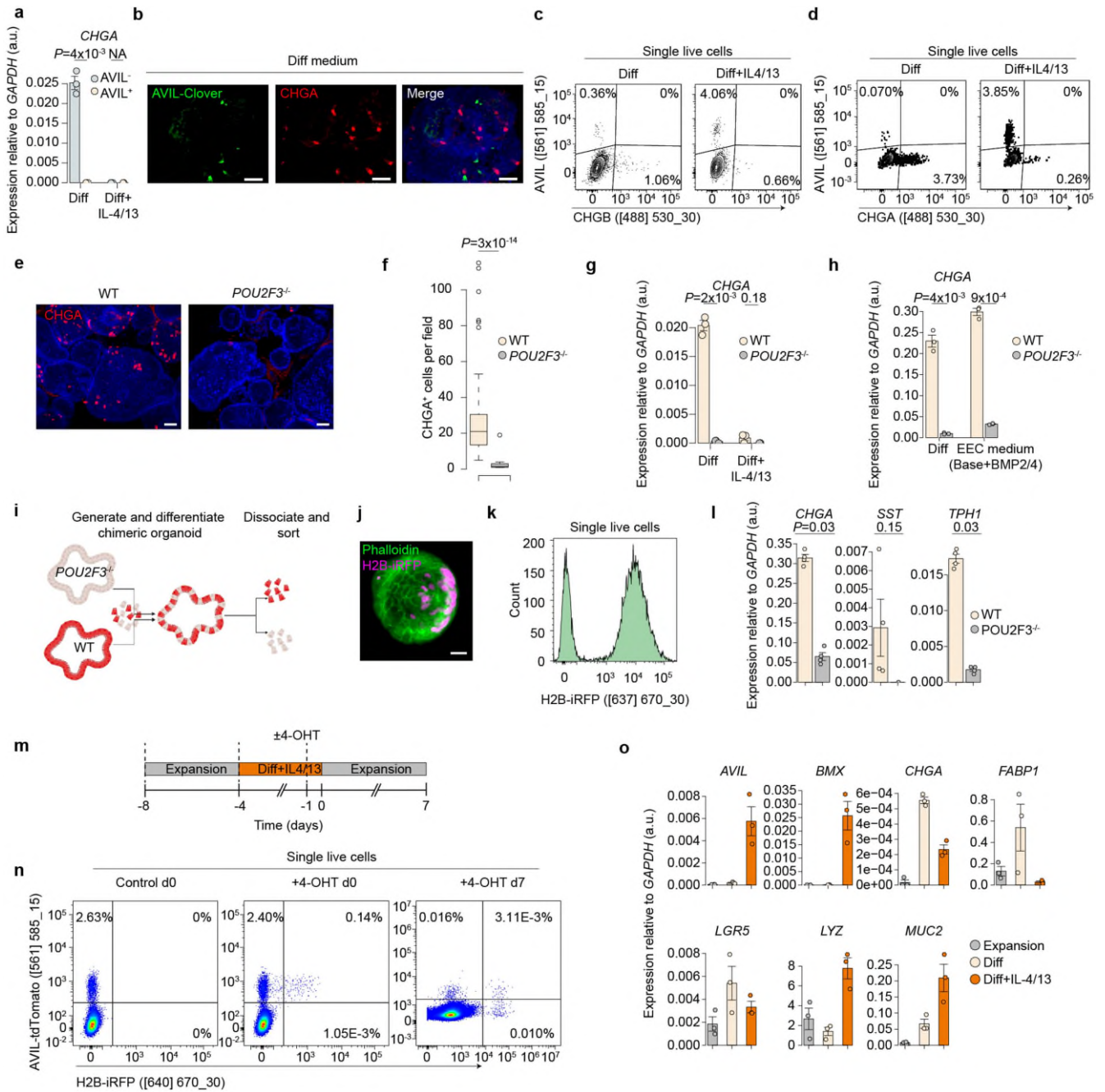
Extended Data Fig. 6 | See next page for caption.

Extended Data Fig. 6 | Human intestinal tuft cell derived organoids.
a, Gating strategy for organoid outgrowth from single S/G2/M phase tuft cell (KIT$^+$) and non-tuft cell (KIT$^-$) sorted from FUCCI reporter organoids differentiated in tuft cell medium with IL-4/IL-13. **b**, Representative images (left) and area quantification (right) of first passage organoids derived from (**a**). n = 47 individual organoids per condition, shown one of three independent experiments (Supplementary Fig. 3a). Boxplot show data from the 25th–75th percentile and whiskers extending to the minimum and maximum within 1.5 × inter-quartile range, with dots marking outliers. **c-d**, Organoid outgrowth from single AVIL$^-$ and AVIL$^+$ cells in AVIL-Clover reporter organoids (**c**), or from single KIT$^-$ and KIT$^+$ cells from human adult duodenum tissue (**d**). **c**, n = 2 donors (Supplementary Fig. 3c). **d**, n = 3 donors (Supplementary Fig. 3b). **e**, qPCR quantification of *LGR5* and *AVIL* expression in sorted AVIL$^-$ and AVIL$^+$ cells at depicted time points following seeding. Each dot is one donor, n = 2 donors. **a-e**, sorted cells were cultured in human expansion medium. **f**, qPCR quantification of intestinal epithelial lineage markers in passage 1 organoids cultured in the depicted regimens. Each dot is one donor, n = 2 donors.

g, Representative images (left) and quantification (right) of different intestinal epithelial cell types in AVIL$^-$ and AVIL$^+$ cell-derived organoids at passage 1. Each dot is an organoid. n = 6 (CHGA), 9 (MUC2), 7 (AVIL) organoids per group from one donor. 3 independent experiments were performed on 2 donors (Supplementary Fig. 3d). **h-i**, qPCR quantification (**h**) and visualization (**i**) of CHGA expression in organoids of passage 4 derived from KIT$^-$ and KIT$^+$ cells as in (**a**). **h**, Each dot is a well. n = 3 wells per condition. 3 independent experiments were performed on two donors with similar results (Supplementary Fig. 3e). **j**, Expression of lineage markers across cell types as in Fig. 3b,c. Left: Dot color relates to mean expression values and dot size to fraction of expressing cells; right: dot color indicates log normalized expression. **k**, Distribution of cell type percentages across medium condition and founder cell. Data are presented as binomial estimation of the mean +/−95% confidence intervals. **j-k**, n = 10,311 single cells. **b-d,g,i**, Scale bar, 500 μm (**b-d**), 20 μm (**g,i**). **e-g,h,k**, Data are presented as mean values (**e,f**) or as mean values +/− standard error (**g,h,k**). **b,g**, P values are derived from two-tailed Student's t-test. Diff: Tuft cell differentiation medium; EEC: Enteroendocrine cells.
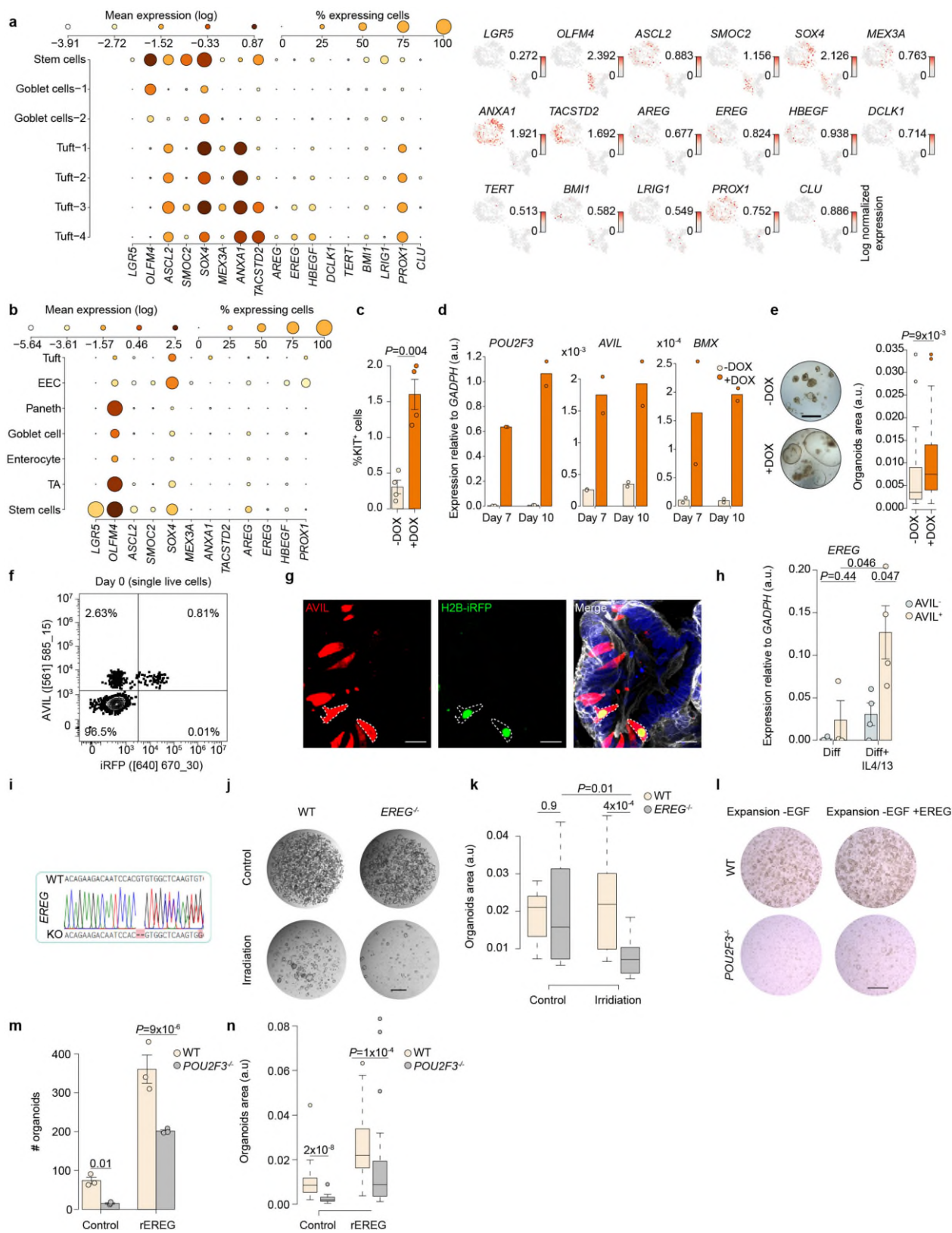
Extended Data Fig. 7 | See next page for caption.

Extended Data Fig. 7 | Lineage tracing of human AVIL⁺ tuft cells. a, qPCR quantification of *CHGA* expression in AVIL⁻ and AVIL⁺ cells sorted from AVIL-Clover reporter organoids. Each dot is a well. Results are pooled from 3 independent experiments on one donor. **b**, CHGA staining in AVIL-Clover reporter organoid. n = 3 independent experiments on the same donor with similar results. **c-d**, Flow cytometric analysis of AVIL and CHGB (**c**) or CHGA (**d**) in human ileum AVIL-P2A-tdtomato/CHGB-mNeon (**c**) and AVIL-P2A-tdtomato/CHGA-Clover (**d**) double reporter organoid lines. 3 independent experiments were performed with similar results. **e-f**, Representative images (**e**) and quantification (**f**) of CHGA⁺ cells in WT and *POU2F3⁻ᐟ⁻* organoids differentiated in tuft cell medium (Diff). Results are pooled from 2 independent experiments on the same donor, n = 76 (WT) and 46 (*POU2F3⁻ᐟ⁻*) individual organoids. Boxplot shows data from the 25th–75th percentile and whiskers extending to the minimum and maximum within 1.5 × inter-quartile range, with dots marking outliers. **g**, qPCR quantification of *CHGA* expression in WT and *POU2F3⁻ᐟ⁻* organoids differentiated in tuft cell differentiation medium with or without IL-4/IL-13. Each dot is a well. n = 3 wells per condition. Experiments were performed on two donors (Supplementary Fig. 3f). **h**, Same as (**g**), organoids were differentiated in either tuft cell or EEC differentiation medium. Each dot is an experiment, n = 3 independent experiments on the same donor.

i-l, i, Schematics of experimental set-up for (**j-l**). Mosaic organoids, derived from *POU2F3⁻ᐟ⁻* and H2B-iRFP wildtype organoid lines, were differentiated for 7 days in tuft cell differentiation medium before sorting. **j-k**, Representative image (**j**) and flow cytometric plot (**k**) of mosaic organoids as in (**i**). **l**, qPCR analysis of enteroendocrine cell markers from sorted H2B-iRFP⁺ and iRFP⁻ (*POU2F3⁻ᐟ⁻*) cells. **j-k**, 2 experiment with similar results. **l**, Each dot is a well. n = 4 wells pooled from 2 experiments. **m-n**, Schematics of experimental set-up (**m**) and flow cytometric plots (**n**) of AVIL lineage tracing organoids. Organoids were differentiated for 4 days in tuft cell medium with IL-4/IL-13, with or without exposure to 1 µM 4-Hydroxytamoxifen (4-OHT) for 20 h, then medium was changed to human intestinal expansion medium. 3 independent experiments were performed with similar results. **o**, qPCR quantification of intestinal epithelial lineage markers in the traced organoids derived from sorted single AVIL⁺iRFP⁺ cells (sorted at day 0 as in **n**). Each dot is an experiment. n = 3 independent experiments. **b,e,j**, Scale bar, 20 µm (**j**), 40 µm (**b, e**). **a,g,h,l,o**, Data are presented as mean values +/− standard error. **a,f-h,l** *P* values are derived from two-tailed Student's t-test. Diff: Tuft cell differentiation medium; WT: wildtype. Schematics in **i** were created using BioRender (J. van Es BioRender.com/v54e687; 2024).

Extended Data Fig. 8 | See next page for caption.

Extended Data Fig. 8 | Regeneration potential of tuft cells following damage.
a-b, Gene-expression profiles of genes associated with adult and repair-induced stem cells in ileum organoids as in Fig. 2a (**a**), or in primary intestinal epithelial cells as in Fig. 1a (**b**). Dot color relates to mean expression values and dot size relates to fraction of expressing cells. **a**, right panel - dot color indicates log normalized expression. **a**, n = 953 cells; **b**, n = 15,184 single cells. **c-d**, Flow cytometric quantification of KIT⁺ cell frequency (**c**) and qPCR quantification of tuft cell genes (**d**) in DOX-triggered *POU2F3* overexpression organoids differentiated in tuft cell medium. Each dot is a well. n = 4 (**c**), 2 (**d**) wells per condition. One of 2 (**d**) or 3 (**c**) independent experiments on the same donor with similar results are shown (Supplementary Fig. 4e,f). **e**, Representative image (left) and quantification of organoid area (right) from *POU2F3* overexpression clonal organoids, with or without DOX inducement. Each dot is an individual organoid, n = 46 (DOX⁻) or 50 (DOX⁺) organoids. Experiments were performed on 2 donors (Supplementary Fig. 4g). **f-g**, Representative flow cytometric analysis (**f**) and fluorescence image (**g**) of AVIL-lineage tracing organoids after irradiation. 3 independent experiments were performed on the same donor with similar results. **h**, qPCR quantification of *EREG* expression in sorted AVIL⁻ and AVIL⁺ cells from human ileum organoids. Each dot is a well, n = 3 (Diff) or 4 (Diff+IL-4/13) biologically replicates. Results are pooled from 2 independent experiments (Supplementary Fig. 4h), **i**, Genotype of human ileum *EREG* knock out organoids. **j-k**, Images (**j**) and quantification of organoid area (**k**) from WT and *EREG*⁻/⁻ organoids exposed to IL-4/13 after irradiation (as in Fig. 4c). **k**, Results are pooled from 2 independent experiments, n = 900 (WT control), 700 (*EREG*⁻/⁻ control), 700 (WT irradiation) and 600 (*EREG*⁻/⁻ irradiation) individual organoids. **l-n**, WT and *POU2F3*⁻/⁻ organoids were differentiated for 7 days in tuft cell differentiation medium with IL-4/IL-13, passaged, then cultured for 7 days in human intestinal expansion medium by removal of EGF, with or without recombinant EREG (rEREG). Shown are representative images (**l**), quantification of organoid numbers (**m**), and organoid areas (**n**). Three independent experiments were performed on 2 donors (Supplementary Fig. 4i). **m**, Each dot is a well. n = 3 wells per condition. **n**, n = 40 (WT control), 20 (*POU2F3*⁻/⁻ control), 40 (WT rEREG) and 40 (*POU2F3*⁻/⁻ rEREG) individual organoids. **e,g,j,l**, Scale bar, 1 mm (**e,j,l**), 20 μm (**g**). **c,d,h,m**, Data are presented as mean values +/− standard error (**c,h,m**) or as mean values (**d**). **e,k,n** Boxplots show data from the 25th–75th percentile and whiskers extending to the minimum and maximum within 1.5 × inter-quartile range, with dots marking outliers. **c,e,h,k,m,n**, *P* values are derived from two-tailed Student's t-test (**c,e,h,k,n**), or two-tailed Mann-Whitney test (**m**). Diff: human tuft cell differentiation medium; WT: wildtype; TA: Transit-Amplifying Cells; EEC: Enteroendocrine cell; DOX: doxycycline.
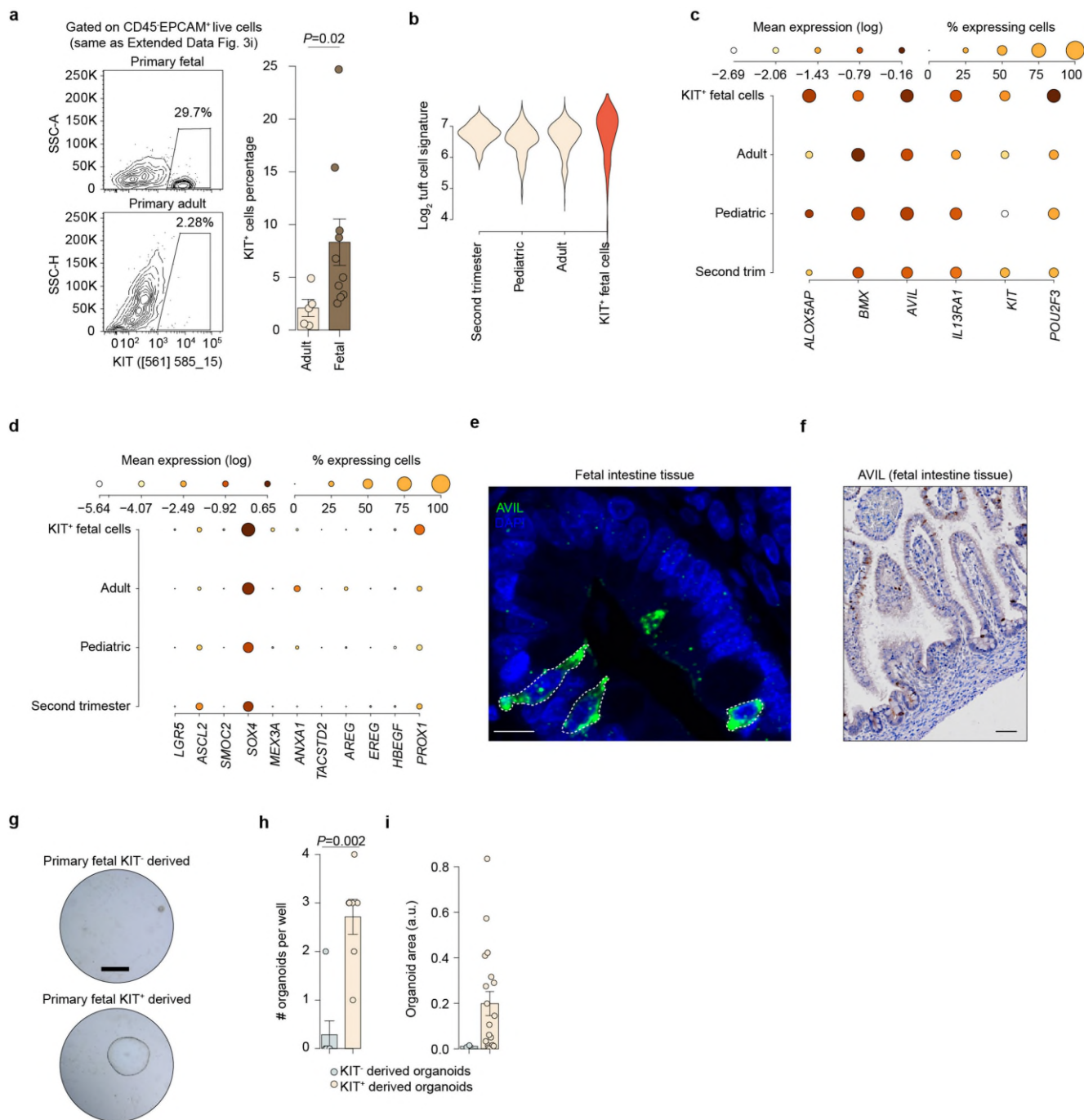
Extended Data Fig. 9 | Analysis of human fetal intestinal tuft cells.
a, Representative flow cytometric plots (left) and quantification (right) of KIT+ cells frequency of human fetal and adult intestinal tissue. Single cells are pre-gated on DAPI⁻CD45⁻EPCAM+. Each dot is a donor. n = 5 (adult), 10 (fetal) donors. **b**, Distribution of a core tuft cell signature across human tuft cells from different development stages[18], as well as within a sorted population of fetal KIT+ cells. The tuft cell signature is as in Extended Data Fig. 3j. **c-d**, Expression of core tuft cells genes (**c**) and genes associated with regenerative stem cells (**d**) across human tuft cells from different development stages, as well as in a sorted population of fetal KIT+ cells. Dot color relates to mean expression

values and dot size to fraction of expressing cells. **b-d**, n = 699 tuft cells, and 89 KIT+ fetal cells. **e-f**, Representative images of AVIL expression in histological sections of human fetal intestine tissue. n = 3 donors with similar results. **g-i**, Representative images (**g**) and quantifications of organoid numbers (**i**) and area (**j**) of organoids derived from single primary fetal (week 19–21) KIT+ and KIT⁻ cells. One of three donors is shown (Supplementary Information Fig. 4j). **h**, Each dot is a well. n = 7 wells per condition. **i**, Each dot is an individual organoid. n = 2 (KIT⁻), 19 (KIT+) organoids. **e,f,g**, Scale bar: 10 μm (**e**), 50 μm (**f**), 500 μm (**g**).**a,h,i**, Data are presented as mean values +/− standard error. **a,h**, P values are derived from two-tailed Student's t-test (**a**) or two-tailed Mann-Whitney test (**h**).

nature portfolio

Corresponding author(s):	Jochem H. Bernink Hans Clevers
Last updated by author(s):	Jul 24, 2024

Reporting Summary

Nature Portfolio wishes to improve the reproducibility of the work that we publish. This form provides structure for consistency and transparency in reporting. For further information on Nature Portfolio policies, see our Editorial Policies and the Editorial Policy Checklist.

Statistics

For all statistical analyses, confirm that the following items are present in the figure legend, table legend, main text, or Methods section.

n/a	Confirmed	
☐	☒	The exact sample size (*n*) for each experimental group/condition, given as a discrete number and unit of measurement
☐	☒	A statement on whether measurements were taken from distinct samples or whether the same sample was measured repeatedly
☐	☒	The statistical test(s) used AND whether they are one- or two-sided *Only common tests should be described solely by name; describe more complex techniques in the Methods section.*
☒	☐	A description of all covariates tested
☐	☒	A description of any assumptions or corrections, such as tests of normality and adjustment for multiple comparisons
☐	☒	A full description of the statistical parameters including central tendency (e.g. means) or other basic estimates (e.g. regression coefficient) AND variation (e.g. standard deviation) or associated estimates of uncertainty (e.g. confidence intervals)
☐	☒	For null hypothesis testing, the test statistic (e.g. *F*, *t*, *r*) with confidence intervals, effect sizes, degrees of freedom and *P* value noted *Give P values as exact values whenever suitable.*
☒	☐	For Bayesian analysis, information on the choice of priors and Markov chain Monte Carlo settings
☒	☐	For hierarchical and complex designs, identification of the appropriate level for tests and full reporting of outcomes
☐	☒	Estimates of effect sizes (e.g. Cohen's *d*, Pearson's *r*), indicating how they were calculated

Our web collection on statistics for biologists contains articles on many of the points above.

Software and code

Policy information about availability of computer code

Data collection	Flow cytometry: BD LSR Fortessa X20 4 laser (BD Biosciences, software FACSDiva v9.0); FACSFusion (BD Biosciences, software FACSDiva v8.0.1), BD FACS Influx (BD Biosciences, BD FACS Software 1.2.0.142) Image and live-cell imaging: Leica SP8 confocal (software LAS X Version 1.1), LS1 Live (Viventis, software version 2.0.0.3), Olympus VS200 slide scanner (Olympus-lifescience, software version VS200 ASW 3.3), Tecnai T12 microscope (Thermo Fisher Scientific, T12), Leica Stellaris8 (Version 4.7.0.28176), LSM 880 (ZEISS, Version ZEN 2). qPCR: Bio-Rad CFX Manager Version 3.1
Data analysis	ImageJ (Fiji, Version 1.51n), ITK-SNAP (version 3.8.0), Microsoft Excel 2016, R Studio (1.1.453), Imaris x64 9.3.1, FlowJo V10.6.2, HandBrake (1.8.1), MetaCell (03.5), STAR (version 2.7.8a), umi_tools (version 1.1.1), ClusterProfiler (version 3.14.0), ChIPpeakAnno (version 3.20.0), Cellranger (version 7.1.0). Custom code and scripts used to analyze the data and produce the figures are available in a public GitHub repository (https://github.com/aygoldberg/TuftOrganoids/).

For manuscripts utilizing custom algorithms or software that are central to the research but not yet described in published literature, software must be made available to editors and reviewers. We strongly encourage code deposition in a community repository (e.g. GitHub). See the Nature Portfolio guidelines for submitting code & software for further information.

Data

All manuscripts must include a data availability statement. This statement should provide the following information, where applicable:

- Accession codes, unique identifiers, or web links for publicly available datasets
- A description of any restrictions on data availability
- For clinical datasets or third party data, please ensure that the statement adheres to our policy

Organoid and primary tissue single-cell RNA-seq data that support the findings of this study were deposited in the Gene Expression Omnibus (GEO) under accession code GSE233451, and are publicly available.
To support the main finding of this paper, we reanalyzed single-cell RNA-seq data from the following sources: The Gut Cell Atlas (https://www.gutcellatlas.org/), https://doi.org/10.5061/dryad.8pk0p2ns8, and Single Cell Portal: SCP259 (https://singlecell.broadinstitute.org/single_cell/study/SCP259/intra-and-inter-cellular-rewiring-of-the-human-colon-during-ulcerative-colitis). Source data are provided with this paper.
Next generation sequencing reads were mapped to the human genome (hg38, https://hgdownload.soe.ucsc.edu/downloads.html#human) .

Research involving human participants, their data, or biological material

Policy information about studies with human participants or human data. See also policy information about sex, gender (identity/presentation), and sexual orientation and race, ethnicity and racism.

Reporting on sex and gender	Both male and female were included.
Reporting on race, ethnicity, or other socially relevant groupings	Researchers were blinded for race, ethnicity or other patient groupings.
Population characteristics	Human fetal intestine tissue and non-inflamed adult intestinal tissue were included. No covariate information on population characteristics is available of obtained donor (adult or fetal) material.
Recruitment	Gestational age, determined by ultrasonic measurement of the diameter of the skull or femur, ranged from 19 to 21 weeks. Uninflamed ileum, duodenum, and colon were obtained from adult patients undergoing tumor–resection surgery; ileal, duodenal and colon tissues were collected at an appropriate distance from the tumor. Resection specimen was obtained as residual material after clinical procedures.
Ethics oversight	Uninflamed ileum, duodenum, and colon were obtained from patients undergoing tumor–resection surgery; tissues were collected at an appropriate distance from the tumor. Resection specimen was obtained as residual material after clinical procedures in accordance with the Declaration of Helsinki, the ethical guidelines of the University Medical Centre Utrecht, Utrecht, and Amsterdam University Medical Centre (AUMC), Amsterdam, the Netherlands. All adult tissue material used in this study was obtained after informed consent, and with approval of tissue-specific protocols by the Medical Ethical Committee of the respective University Medical Centers. Human fetal tissue was obtained from elective abortions at the Stichting Bloemenhove clinic in Heemstede, the Netherlands, upon on the receipt of informed consent. The use of human abortion tissues was approved by the Medical Ethical Committee of the Academic Medical Center, Amsterdam, the Netherlands. Gestational age, determined by ultrasonic measurement of the diameter of the skull or femur, ranged from 19 to 21 weeks.

Note that full information on the approval of the study protocol must also be provided in the manuscript.

Field-specific reporting

Please select the one below that is the best fit for your research. If you are not sure, read the appropriate sections before making your selection.

☒ Life sciences ☐ Behavioural & social sciences ☐ Ecological, evolutionary & environmental sciences

For a reference copy of the document with all sections, see nature.com/documents/nr-reporting-summary-flat.pdf

Life sciences study design

All studies must disclose on these points even when the disclosure is negative.

Sample size	No sample size calculation was performed. The sample sizes used were in the same range of other studies in the field (Beumer J, et al. Cell. 2020 Aug 20;182(4):1062-1064; Lorenzo-Martín, L.F., et al. Nature 629, 450–457 (2024)). The organoid lines were derived from 5 individual donors used in this study. The exact n numbers are indicated in each legends.
Data exclusions	In SORT-seq single cell analysis (Fig. 2), cells with less than 500 UMI or more than 40% mitochondrial transcripts were excluded. In 10x single cell analysis (Fig. 3), single cells with less than 64 UMI of a specific cellplex barcode were discarded from down-stream analysis. Single cells with less than 8-fold UMI count ratio between highest and second highest cellplex barcodes were marked as doublets and discarded from down-stream analysis. Single cells with less than 1,000 genomic UMIs or more than 20% mitochondrial content failed to pass QC and were discarded from further analysis.

	In all other experiments, no data points were excluded.
Replication	All experiments were performed in multiple distinct replicates, in several organoid lines from different donors if applicable, as indicated in the text and figure legends.
Randomization	Organoids to be analyzed were chosen randomly.
Blinding	In single cell analysis, researchers were blinded to cell source (e.g., gating or culture conditions). In other experiments, researchers were not blinded for treatment or organoid genotypes, as it is not common practice in the field (Lorenzo-Martín, L.F., et al. Nature 629, 450–457 (2024)), and in order to avoid mix-up of samples. All different samples were treated in the exact same manner with proper controls, to assure accuracy and reproducibility of measurements and analysis.

Reporting for specific materials, systems and methods

We require information from authors about some types of materials, experimental systems and methods used in many studies. Here, indicate whether each material, system or method listed is relevant to your study. If you are not sure if a list item applies to your research, read the appropriate section before selecting a response.

Materials & experimental systems

n/a	Involved in the study
☐	☒ Antibodies
☐	☒ Eukaryotic cell lines
☒	☐ Palaeontology and archaeology
☒	☐ Animals and other organisms
☒	☐ Clinical data
☒	☐ Dual use research of concern
☒	☐ Plants

Methods

n/a	Involved in the study
☒	☐ ChIP-seq
☐	☒ Flow cytometry
☒	☐ MRI-based neuroimaging

Antibodies

Antibodies used	The following antibodies (clone, dilution, supplier, catalogue number, Lot number) were used in flow cytometry: PE anti-human CD117 antibody (KIT, clone 104D2, 1:100, Biolegend, #313204, Lot B141912), Biotin anti-human CD117 (clone 104D2, 1:100, Biolegend, #313208, Lot B283575), Alexa Fluor 488 anti-human CD326 (Epcam, clone 9C4, 1:100, Biolegend, #324210, Lot B352438), APC/Cy7 anti-human CD45 (clone HI30, 1:100, Biolegend, #304014, Lot B145995, Lot B355047). Secondary antibody: Brilliant Violet 421™ Streptavidin (1:1000, Biolegend, #405226, Lot B344430). Antibodies used in immunohistochemistry and immunofluorescence stainings: anti-AVIL (rabbit polyclonal, 1:500 for immunohistochemistry, 1:300 for immunofluorescence staining, Sigma-Aldrich, #HPA058864, Lot 000047314), anti-GFP (goat polyclonal, 1:600, Abcam, #ab6673, Lot 1033180-6), mouse anti-KI67(clone MM1, 1:4000 used in immunohistochemistry staining, Monosan, #MONX10283, Lot 45X10283J), mouse anti-KI67 (clone B56, 1:100, BD Pharminge, #550609, Lot 2052205), anti-chromogranin A (rabbit polyclonal, 1:600 in immunohistochemistry staining, 1:100 used in immunofluorescence staining, labned.com, #LN1401487, no lot number available), rabbit anti-mucin 2 (clone H-300, 1:200, santa cruz biotechnology, #sc-15334, Lot E1513), anti-APOB (rabbit polyclonal, 1:100, Novus biologicals, #NBP2-38608, Lot A118682), anti-POU2F3 (rabbit polyclonal, 1:100, Sigma-Aldrich, #HPA019652, no lot number available), anti-Lysozyme (rabbit polyclonal, 1:100, GeneTex, #GTX72913, Lot 822004521), rabbit anti-Vimentin (clone D21H3, 1:100, Cell Signaling technology, #5741S, Lot 1), mouse anti-TM4SF4 antibody (clone 4E6, 1:100, Sigma-Aldrich, #sc-293348, Lot F1818), APC Mouse anti-human CD274 (clone MIH1, 1:100, BD Pharmingen, #563741, Lot 9262207), anti-GNAT3 (goat polyclonal, 1:100, LSBio, #LS-B4942, Lot 65974), anti-GNAT3 (goat polyclonal, 1:500, Aviva Systems biology, #OAEB00418, No lot available), anti-CD117 (c-kit, rabbit polyclonal, 1:100, DAKO, #A4502, Lot 11402117). Secondary antibodies for immunohistochemistry: goat anti-rabbit HRP (ready to use, Immunologic, #DPVR110HRP, Lot 180822) or EnVision kits anti-mouse (ready to use, Dako, #K4001, Lot 11370011). Secondary antibodies for immunofluorescence stainings were all bought from Thermo Fisher, dilution 1:1000. Alexa Fluor 405 donkey anti-rabbit, #A48258, Lot YD369488; Alexa Fluor 488 donkey anti-mouse, #A21202, Lot 2428531; Alexa Fluor 488 donkey anti-goat, #A11055, Lot 2465077; Alexa Fluor 568 donkey anti-rabbit, #A10042, Lot 2433862; Alexa Fluor 647 goat anti-mouse, #A21236, Lot 2382182; Alexa Fluor 647 donkey anti-rabbit, #A31573, Lot 2420695; Donkey anti-Rabbit IgG (H+L) Cross-Adsorbed Secondary Antibody, DyLight™ 755, #SA5-10043, Lot YH4030241. F-actin was visualized by staining with Alexa Fluor 488 Phalloidin (Thermo Fisher Scientific, 1:1000, #A12379, Lot 2738393) or Phalloidin–Atto 647N (1:1000, Sigma-Aldrich, #65906, Lot BCCK9313).
Validation	All antibodies listed in the previous section were validated by the manufacture and/or by previous studies. The information on the validation of antibodies for flow cytometry can be found as stated below: Biolegend antibodies: https://www.biolegend.com/en-us/quality/quality-control Biolegend did specificity testing of 1-3 target cell types with either single- or multi-color analysis (including positive and negative cell types). Once specificity is confirmed, each new lot must perform with similar intensity to the in-date reference lot. Brightness (MFI) is

evaluated from both positive and negative populations. Each lot product is validated by QC testing with a series of titration dilutions.

The information on the validation of primary antibodies for immunohistochemistry and immunofluorescence stainings as listed below:

Rabbit anti-human AVIL, (https://www.sigmaaldrich.com/NL/en/product/sigma/hpa058864?icid=sharepdp-clipboard-copy-productdetailpage). Application includes immunohistochemistry (IHC). Validated by the Human Protein Atlas (HPA) project, IHC tissue array of 44 normal human tissues and 20 of the most common cancer type tissues. Protein array of 364 human recombinant protein fragments. The specificity of this antibody also validated by staining in AVIL-Clover knock-in reporter in human intestinal organoids derived from 4 different donors in this manuscript. Citations: e.g. PMID: 32483224, PMID: 30221190.

Goat anti-GFP, reacts with GFP-tag samples (https://www.abcam.com/en-nl/products/primary-antibodies/gfp-antibody-ab6673). Applications used include IHC, IHC-IF, WB and IF. Validated by abcam in IP, ELISA, WB, IF, IHC-P, ICC/IF, IHC-Fr, IHC-FrFl and tested in Tag, Tag-Aequorea victoria samples. Cited in 692 publications, all listed on the website (https://www.citeab.com/antibodies/732941-ab6673-anti-gfp-antibody).

Mouse anti-KI67, reacts with human, (https://www.monosan.com/catalog/product/view/id/1550221). Applications: IHC-P, IHC. Cited in 11 publications, all available on the website (https://www.citeab.com/antibodies/13956705-monx10283-anti-ki67-antigen-clone-mm1-monoclonal), e.g. PMID: 38023731, PMID: 34433038.

Mouse anti-KI67, reacts with human (QC Testing by BDBiosciences), Mouse (Tested in Development by BDBiosciences), Rat,Rhesus (Reported), (https://www.bdbiosciences.com/en-us/products/reagents/flow-cytometry-reagents/research-reagents/single-color-antibodies-ruo/purified-mouse-anti-ki-67.550609). Application: Flow cytometry (Routinely Tested by BDBiosciences), Immunohistochemistry-formalin (antigen retrieval required), Immunohistochemistry-frozen (Tested by BDBiosciences During Development). Cited in 820 publications, all available on this website (https://www.citeab.com/antibodies/2412437-550609-bd-pharmingen-purified-mouse-anti-ki-67).

Rabbit anti-CHGA, reacts with human, mouse. No lot number available. Application: IHC and IF. Validated by staining in CHGA-mNEON knock-in reporter line in human intestine organoids showed in other study (PMID: 32123335). Also cited in PMID: 30712869, PMID: 32123335.

Rabbit anti-mucin 2 , reacts with mouse, rat and human, https://datasheets.scbt.com/sc-15334.pdf. Applications: Mucin 2 (H-300) is recommended by Santa Cruz Biotechnology for detection of Mucin 2 by immunofluorescence and immunohistochemistry. Validated by Santa Cruz Biotechnology: Immunofluorescence staining of methanol-fixed SW480 cells showing cytoplasmic localization; immunoperoxidase staining of formalin fixed, paraffin-embedded human colon tissue showing cytoplasmic staining of glandular cells. Cited in 346 publications, all available on the company website (https://www.citeab.com/antibodies/815800-sc-15334-mucin-2-antibody-h-300).

Rabbit anti-APOB, reacts with human, (https://www.novusbio.com/products/apolipoprotein-b-apob-antibody_nbp2-38608). Validated by novusbio company, Apolipoprotein B/ApoB staining in Human HepG2 cell lines shows localization to cytosol and vesicles, applications in ICC/IF, IHC. Citation: e.g. PMID: 35583599.

Rabbit anti-POU2F3, reacts with human, (https://www.sigmaaldrich.com/NL/en/product/sigma/hpa019652).The antibody was validated by Human Protein Atlas (HPA) project and by western blot and immunoprecipitation of overexpressed Flag-tagged POU2F3 in HEK293T cells in the paper PMID: 35576971. Applications: western blotting, immunofluorescence and immunohistochemistry. Cited in 14 publications (https://www.citeab.com/antibodies/1520962-hpa019652-anti-pou2f3-antibody-produced-in-rabbit): e.g. PMID: 38676800, PMID: 35576971, PMID: 34880874.

Rabbit anti- Lysozyme, reacts with human, (https://www.genetex.com/Product/Detail/Lysozyme-antibody/GTX72913). Validated by GeneTex company: This antibody reacts with lysozyme. It stains granulocytes, monocytesand macrophages in human tonsil, skin and colon. This antibody does not cross-react with any other cell types. Application: IHC-P. Cited in 4 publications, all available on the website, e.g. PMID: 30526881, PMID: 32917713.

Rabbit anti-Vimentin, reacts with Human, Mouse, Rat, Hamster, Monkey, Virus, Mink, Chicken , D. melanogaster, Xenopus, Zebrafish, Bovine, Dog, Pig, S. cerevisiae, C. elegans, Horse, Guinea Pig, (https://www.cellsignal.com/products/primary-antibodies/vimentin-d21h3-xp-rabbit-mab/5741). Validated by Cell Signaling Technology: Western blot analysis of extracts from control HeLa cells or Vimentin knockout HeLa cells using Vimentin (D21H3) XP Rabbit mAb or β-Actin,Rabbit mAb. The absence of signal in the Vimentin knockout HeLa cells confirms specificity of the antibody for Vimentin. Applications: Western Blot, Immunoprecipitation, Immunohistochemistry, Chromatin Immunoprecipitation, Immunofluorescence, Flow Cytometry. Cited in 2751 publications, all available on the website, e.g. PMID: 38135696.

Mouse anti-TM4SF4 antibody, reacts with human, (https://ct-uat2.scbt.com/p/tm4sf4-antibody-4e6), validated by Santa Cruz Biotechnology using Western blot analysis of TM4SF4 expression in non-transfected and TM4SF4 transfected 293T whole cell lysates, positive signal only was in transfected cell lysates. Applications: recommended Santa Cruz Biotechnology for detection of TM4SF4 of human origin by WB, IP and ELISA. Cited in PMID: 35456465.

APC Mouse anti-human CD274, (https://www.bdbiosciences.com/en-us/products/reagents/flow-cytometry-reagents/research-reagents/single-color-antibodies-ruo/apc-mouse-anti-human-cd274.563741). Validation by BDBiosciences using flow cytometric analysis of human CD274 expression by CD274-transfected Jurkat cells. Applications: FC/FACS. Cited in 21 publications, all available on the website (https://www.citeab.com/antibodies/2407788-563741-apc-mouse-anti-human-cd274), e.g. PMID: 37900310, PMID: 37509655.

Goat anti-GNAT3 antibody, reacts with Human, Monkey, Mouse, Rat, Bovine, Dog, Hamster, Horse, Pig, Rabbit, (https://www.lsbio.com/antibodies/ihc-plus-gnat3-antibody-gustducin-antibody-aa304-318-ihc-ls-b4942/128352). Validated by LSBio company for IHC and Peptide-ELISA, tested on 20 paraffin-embedded human tissues. Applications: IHC, IHC-P, Peptide-ELISA. Cited in

PMC4305516, PMC8623908.

Goat anti- GNAT3 antibody, reacts with Human, Mouse, Rat, (https://www.avivasysbio.com/gnat3-antibody-oaeb00418.html). Validated by Aviva Systems Biology by staining of paraffin embedded Human Small Intestine. Applications used include IHC, ICC, IHC-IF, and WB. Cited in 13 publications, all available on the website (https://www.citeab.com/antibodies/1005837-oaeb00418-gnat3-antibody-oaeb00418), e.g. PMID: 28316078, PMID: 29778504.

Rabbit anti-CD117 (c-kit) antibody, reacts with Human, (https://www.agilent.com/en/product/immunohistochemistry/antibodies-controls/primary-antibodies/cd117-c-kit-(concentrate)-76145). Validation: In Western blotting of an extract of the small cell lung carcinoma cell line SY, that over-expresses c-kit mRNA, the antibody labels a band of 145 kDa corresponding to the c-kit protein. The labeled band is rather broad, from 120 to 155 kDa. An additional band of 100 kDa is also labeled. In another study applying a different antibody to c-kit, a 100 kDa protein was, likewise, labeled. This labeling was abolished when the antibody was incubated with the synthetic c-kit peptide antigen used for immunization. In Western blotting, the antibody did not react with an extract of the adenocarcinoma cell line HS, that is without c-kit gene expression. Application: IHC, WB, IHC-IF, IF. Cited in 558 publications, all available on the company website (https://www.citeab.com/antibodies/3382892-a4502-cd117-c-kit), e.g. PMID: 38610874, PMID: 38173156.

Eukaryotic cell lines

Policy information about cell lines and Sex and Gender in Research

Cell line source(s)	All human adult intestine organoid lines were derived from resection specimen which are obtained as residual material after clinical procedures in accordance with the Declaration of Helsinki, the ethical guidelines of the University Medical Centre Utrecht, Utrecht, and Amsterdam University Medical Centre (AUMC), Amsterdam, the Netherlands. donor 1, human ileum organoid line, male; donor 2, human duodenum organoid line, male; donor 3, human ileum organoid line, female; donor 4, human colon organoid line, female; donor 5, human colon organoid line, male.
Authentication	None of the organoid lines were authenticated.
Mycoplasma contamination	All organoid lines were regularly assessed for mycoplasma contamination and scored negatively without exception.
Commonly misidentified lines (See ICLAC register)	No commonly misidentified cell lines were used.

Plants

Seed stocks	*Report on the source of all seed stocks or other plant material used. If applicable, state the seed stock centre and catalogue number. If plant specimens were collected from the field, describe the collection location, date and sampling procedures.*
Novel plant genotypes	*Describe the methods by which all novel plant genotypes were produced. This includes those generated by transgenic approaches, gene editing, chemical/radiation-based mutagenesis and hybridization. For transgenic lines, describe the transformation method, the number of independent lines analyzed and the generation upon which experiments were performed. For gene-edited lines, describe the editor used, the endogenous sequence targeted for editing, the targeting guide RNA sequence (if applicable) and how the editor was applied.*
Authentication	*Describe any authentication procedures for each seed stock used or novel genotype generated. Describe any experiments used to assess the effect of a mutation and, where applicable, how potential secondary effects (e.g. second site T-DNA insertions, mosiacism, off-target gene editing) were examined.*

Flow Cytometry

Plots

Confirm that:

☒ The axis labels state the marker and fluorochrome used (e.g. CD4-FITC).

☒ The axis scales are clearly visible. Include numbers along axes only for bottom left plot of group (a 'group' is an analysis of identical markers).

☒ All plots are contour plots with outliers or pseudocolor plots.

☒ A numerical value for number of cells or percentage (with statistics) is provided.

Methodology

Sample preparation	Human adult intestinal organoids were dissociated into single cells using TrypLE (TrypLE Express, Life Technologies, cat. no.12605036) with 10 µM Rho kinase inhibitor (RhoKi, Abmole, cat. no. Y-27632) in 37°C and mechanical disruption by pipetting every 5 minutes. Cells were sorted direclty (e.g. reporter cell lines) or stained 30 mins with antibody on ice, or incubated 15 mins at RT with 100 µl Cell Multiplexing Oligo, After wash, cells were analyzed or sorted using flow cytometry.

To obtain single cells from human primary fetal and adult intestinal tissue, the tissue were minced into small pieces of ~1 mm3 and digested 30-45 min in 5 mg/ml collagenase type II (Sigma Aldrich, cat. no. C9407-1) with 10 µM RhoKi. Then the cells were filtered and stained before sorting.

Instrument

BD LSR Fortessa X20 4 laser (BD Biosciences) was used for cell analysis; BD FACSAria Fusion (BD Biosciences), BD FACS Influx (BD Biosciences) were used for cell sorting.

Software

Software for data collection: BD LSR Fortessa X20 4 laser (FACSDiva v9.0); FACSFusion (FACSDiva v8.0.1), BD FACS Influx (BD FACS Software 1.2.0.142)
Software for data analysis: FlowJo V10

Cell population abundance

The human intestinal tuft cells were sorted using AVIL reporter organoids, then identified by single cell RNA-sequence as shown in figures. Primary human intestinal tuft cells identified by KIT+ epithelial cells, the purity was >97% across multiple donors identified by single cell RNA-sequence. For organoids and primary human cell analysis and sorting, population abundance as indicated on the plots and graphs.

Gating strategy

Cells were identified based on FSC and SSC gating.Single cells were identified as is shown in the gating strategies included in the extended data figure 1a, briefly:
1: SSC-A/FSC-A
2: FSC-H/FSC-A
3: SSC-H/SS-A
4: DAPI live cell staining and selecting the DAPI- population
5: Analysis of the fluorophores

Boundaries are defined based on comparison with the negative controls:
mClover, mNeon, tdtomato and H2B-iRFP positive cells were identified as positive based on comparison to non-reporter organoid lines. For traced positive cells from tamoxifen treated lineage tracing organoid line were identified as positive based on comparison to non-tamoxifen treated organoids.

For primary human cells, cells were gated as above for size and singlets and then for live cells (DAPI- cells) and CD45 negative, Epcam postivite cells based on CD45, Epcam ab staining prior to gating on KIT (CD117) staining as shown.
Full gating strategies are included in the extended data figures.

☒ Tick this box to confirm that a figure exemplifying the gating strategy is provided in the Supplementary Information.